

Gated Domain Units for Multi-source Domain Generalization

Simon Föll^{1*} Alina Dubatovka^{2*} Eugen Ernst^{3†} Siu Lun Chau^{5†} Martin Maritsch¹
 Patrik Okanovic² Gudrun Thäter³ Joachim M. Buhmann² Felix Wortmann^{1,4}
 Krikamol Muandet⁵

¹Department of Management, Technology, and Economics, ETH Zurich, Switzerland

²Department of Computer Science, ETH Zurich, Switzerland

³Department of Mathematics, Karlsruhe Institute for Technology, Germany

⁴Institute for Technology Management, University of St. Gallen, Switzerland

⁵CISPA - Helmholtz Center for Information Security, Germany

sfoell@ethz.ch alina.dubatovka@inf.ethz.ch euernst@kit.edu siu-lun.chau@cispa.de
 mmaritsch@ethz.ch pokanovic@ethz.ch gudrun.thaeter@kit.edu jbuhmann@inf.ethz.ch
 felix.wortmann@unisg.ch muandet@cispa.de

Abstract

The phenomenon of distribution shift (DS) occurs when a dataset at test time differs from the dataset at training time, which can significantly impair the performance of a machine learning model in practical settings due to a lack of knowledge about the data’s distribution at test time. To address this problem, we postulate that real-world distributions are composed of latent *Invariant Elementary Distributions* (I.E.D) across different domains. This assumption implies an invariant structure in the solution space that enables knowledge transfer to unseen domains. To exploit this property for domain generalization, we introduce a modular neural network layer consisting of Gated Domain Units (GDUs) that learn a representation for each latent elementary distribution. During inference, a weighted ensemble of learning machines can be created by comparing new observations with the representations of each elementary distribution. Our flexible framework also accommodates scenarios where explicit domain information is not present. Extensive experiments on image, text, and graph data show consistent performance improvement on out-of-training target domains. These findings support the practicality of the I.E.D assumption and the effectiveness of GDUs for domain generalisation.

1 Introduction

Machine learning relies on the fundamental assumption that training and test data are independently and identically distributed (I.I.D.), which ensures the learning machine attains the lowest achievable risk as the sample size grows under the empirical risk minimization (ERM) framework (Vapnik, 1998; Schölkopf, 2019). However, numerous research and real-world applications (Zhao et al., 2018; 2020; Ren et al., 2019; Taori et al., 2020) have provided staggering evidence against this assumption; as shown in D’Amour et al. (2020). In practice, the I.I.D. assumption is often violated due to distribution shift (DS), which occurs where a model is applied to a dataset that differs from its training data (Sugiyama & Kawanabe, 2012), resulting in significantly impaired performance.

To tackle DS, recent work advocates for domain generalization (DG): Given data from multiple domains, e.g., Continental Europe hospitals, how to train a model that can generalize well to unseen domains, e.g., US hospital? (Blanchard et al., 2011; Muandet et al., 2013; Zhou et al., 2021a). The ability to generalize to entirely new domains is crucial for the robust and safe deployment of machine learning models, particularly when

*These authors contributed equally.

†These authors contributed equally.

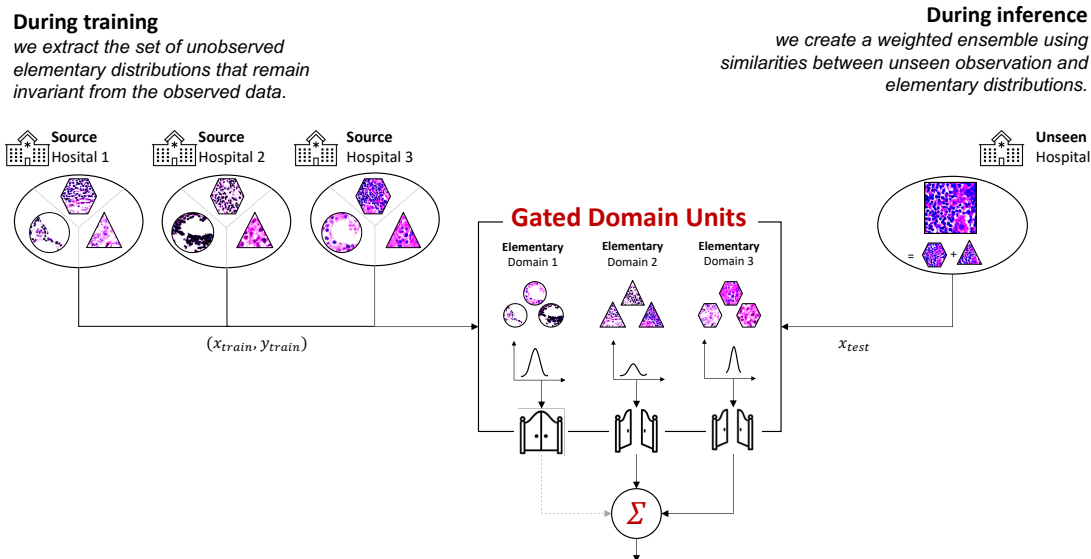


Figure 1: An illustration of invariant elementary distributions in *camelyton17* dataset and the concept of the Gated Domain Units (GDUs). While data sources are often considered as domains, each hospital contains heterogeneous subsets that are shared across sources. We can depict examples of these subsets (latent domains) in three different shapes (rectangle, octahedron, and circle) for each domain following the method of Matsuura & Harada (2020). In contrast to existing work, the invariant elementary distribution (I.E.D.) assumption advocates that these latent domains remain invariant across the hospitals. Therefore, we propose to learn representations of these elementary domains akin to mixture models, and utilise our Gated Domain Units to build a weighted ensemble during inference time.

unforeseeable domains arise after deployment. Nevertheless, the question of how to identify the appropriate *invariance* that enables such generalization remains an open and unresolved issue, as noted by Gulrajani & Lopez-Paz (2020).

In the following, we introduce two examples from Koh et al. (2021) to challenge common assumptions of domain definitions from the well-established benchmark for DG. In *camelyon17* (Bánci et al., 2019), the task is to train a model to classify a tumor (i.e., benign or malignant) based on images of tissue slices from a few hospitals and test the model on an unseen hospital. Here, each hospital is considered a domain. However, when studying tissue slices under a microscope, the source of variation arises from differences in patient population, slide staining, and image acquisition, and thus not necessarily from the hospital itself Veta et al. (2016); Komura & Ishikawa (2018); Tellez et al. (2019). Further, in *OGB-MolPCBA* (Hu et al., 2021), the task is to predict the biochemical properties of small molecules from a set of possible molecules and generalize to a set of molecules structurally different from those seen in the training set. Each scaffold (i.e., subset of structurally similar molecules) is considered a domain, thus yielding over 120,000 domains in *OGB-MolPCBA*. Though the definition of domains is bio-chemically motivated, this assumption causes computation overhead, making it challenging to find an invariance across these scaffolds.

Prior work has made a similar motivation to advocate for learning so-called latent domains in the combined source dataset through an unsupervised manner Deecke et al. (2022); Matsuura & Harada (2020); Chen et al. (2022). The motivation is to become independent of domain labels, when applying DG that learn an invariant structure across domains during training (see Section 2 for a discussion). However, this line of work does not draw a connection between the latent source domains and test domains. In contrast, our paper follows the current trend in DG research that establishes connections between test-time and source domains. Unlike previous work that assumes test-time domains are convex combinations of source domains, we propose that both domains are linear combinations of some latent invariant units, which can be learned during training. This assumption, formally introduced in Definition 1, induces an invariant structure in the

hypothesis space, which are practically appealing for domain generalization (cf. Proposition 3.1). To turn theory into practice, we develop a neural network layer consisting of gated domain units (GDUs) that learn a geometric representation of each elementary domains in the form of kernel mean embedding (KME) (Berlinet & Thomas-Agnan, 2004; Smola et al., 2007; Muandet et al., 2017). During inference, a weighted ensemble of learning machines can be created by comparing new observations with the elementary domains embeddings. We depicted our idea in Figure 1.

We summarise our contributions as follows:

1. We propose the Invariant Elementary Distribution (I.E.D) assumption, postulating both test-time and source domains consist of latent elementary distributions that can be learned during training, and show the assumption’s practical appeal for domain generalization.
2. We develop a modular neural network layer consisting of Gated Domain Units, each captures and learns an elementary distribution via kernel mean embeddings. These representations can thus be used to adapt the ensemble weights to an unseen domain at test time.
3. We verify the I.E.D assumption by extensive experiments using a publicly available benchmarking WILDS. Specifically, we validate our method on image, text, and graph datasets, showing consistent improvement on out-of-training target domains.
4. We provide an effective TensorFlow and PyTorch implementation applicable to different feature extractors such as ResNet50, DistillBERT, and GIN virtual and thus a broad audience of researchers and practitioners to enable a fast adaption of our method.

The remainder of this paper is organized as follows: Section 2 outlines related work, and lays out research gaps that we aim to address. Our theoretical framework is presented in Section 3, followed by our modular DG layer implementation shown in Section 4. Our experimental evaluations are then presented in Section 5. Finally, we discuss the potential limitations and future work in Section 6.

2 Previous Work and Motivation

DG, also known as out-of-distribution (OOD) generalization, is among the hardest problems in machine learning (Blanchard et al., 2011; Muandet et al., 2013; Arjovsky et al., 2019). In contrast, domain adaptation (DA), which predates DG and OOD problems, deals with a slightly simpler scenario in which some data from the test distribution are available (Ganin et al., 2015). Hence, based on the available data, the task is to develop learning machines that transfer knowledge learned in a source domain specifically to the target domain. Approaches pursued in DA can be grouped primarily into (1) discrepancy-based DA (Sun et al., 2016; Peng & Saenko, 2018; Ben-David et al., 2010; Fang et al., 2020; Tzeng et al., 2014; Long et al., 2015) (2) adversary-based DA (Tzeng et al., 2017; Liu & Tuzel, 2016; Ganin et al., 2015; Long et al., 2018), and (3) reconstruction-based DA (Bousmalis et al., 2016; Hoffman et al., 2018b; Kim et al., 2017; Yi et al., 2017; Zhu et al., 2017; Ghifary et al., 2014). In DA, learning the domain-invariant components requires access to unlabeled data from the target domain. Unlike problems in DA, where the unlabeled data from the test domains is accessible to find the right invariant structures (Ben-David et al., 2010), the lack thereof in DG calls for a *postulation* of invariant structure that will enable the OOD generalization (Gulrajani & Lopez-Paz, 2020).

To enable generalization to unseen domains without any access to data from them, researchers have made significant progress in the past decade and developed a broad spectrum of methodologies (Zhou et al., 2021a;b; Li et al., 2019; Blanchard et al., 2011). For thorough review see, e.g., Zhou et al. (2021a); Wang et al. (2021). Existing works can be categorized into methods based on domain-invariant representation learning (Muandet et al., 2013; Li et al., 2018b;c), meta-learning (Li et al., 2018a; Balaji et al., 2018), data augmentation (Zhou et al., 2020), to name a few. Another recent stream of research from a causal perspective includes invariant risk minimization (Arjovsky et al., 2019), invariant causal prediction (Peters et al., 2016), and causal representation learning (Schölkopf et al., 2021). The overall motivation here is to learn the representation that is robust to domain-specific spurious correlations. In other words, it is postulated that “causal” features

are the right kind of invariance that will enable OOD generalization. On the other hand, latent domain discovery is another popular approach in DG. Finding pseudo-domains through an unsupervised manner allows one to learn invariant feature extractors across such latent domains (Hoffman et al., 2012; Li et al., 2020; Gong et al., 2013; Matsuura & Harada, 2020). This line of work is practically appealing when collecting explicit domain labels are difficult in practice, as discussed in Appendix B.2.

Finally, ensemble learning has been shown to be effective in DG (Wang et al., 2021). A particular branch of ensemble learning is domain-specific models, which aim to learn a source domain-specific model, i.e., models specializing in each source domain (Piratla et al., 2020; Monteiro et al., 2021). To avoid redundancy, domain-specific models share some shallow layers of the network that capture generic features. At inference time, predictions can either be averaged or selected based on additional models that predict the similarity of a test observation to a source domain. However, these domain-specific models require domain labels to train the domain classifiers and additional models, making it challenging to integrate the approach into a holistic and efficient framework. Further, these approaches have not been combined with the idea of latent elementary domains.

Motivation. The focus of our work is to address two challenges that we have identified within latent domain approaches. The first challenge is that previous work has not taken into account the invariance of latent representations between source domains and test domains, which limits their effectiveness for test-time adjustments and adaptation. The second challenge is the lack of effective architectures for these approaches, particularly ones that can be easily integrated into existing deep learning frameworks. Practitioners require methods that can handle feature extractors for various data types, such as ResNet-50 (He et al., 2016), DenseNet-121 (Huang et al., 2017), Graph Isomorphism Networks with virtual nodes (GIN-virtual; Xu et al., 2019) and Gilmer et al. (2017)), DistillBERT (Sanh et al., 2020), with minimal integration effort. In our work, we propose the "invariant elementary distributions" assumption to tackle the first challenge, and we propose an effective layer consisting of Gated Domain Units to address the second challenge. More details on this can be found in the next two sections.

3 Domain Generalization with Invariant Elementary Distributions

We leverage the above observation for domain generalization by considering the *mixture component shift* - the most common form of DS - which states that the data is made up of different sources, each with its own characteristics, and their proportions vary between domains (Quinero-Candela et al., 2022, pp. 19).

3.1 Invariant Elementary Distributions

Let \mathcal{X} and \mathcal{Y} be the input and output space, with a joint distribution \mathbb{P} . Let X and Y be random variables taking values in \mathcal{X} and \mathcal{Y} , respectively. We are given a set of D labeled source datasets $\{\mathcal{D}_i^s\}_{i=1}^D$ with $\mathcal{D}_i^s \subseteq \mathcal{X} \times \mathcal{Y}$. Each of the source datasets is assumed to be I.I.D. generated by a joint distribution \mathbb{P}_i^s with support on $\mathcal{X} \times \mathcal{Y}$, henceforth denoted *domain*. Note that the conditional distributions of different domains may change. Hence, our work differs from related work in DG that rely on the covariate shift assumption, i.e., the conditional distribution of the training and test data stays the same (David et al., 2010). The set of probability measures with support on $\mathcal{X} \times \mathcal{Y}$ is denoted by \mathcal{P} . The multi-source dataset \mathcal{D}^s comprises the merged individual source datasets $\{\mathcal{D}_j^s\}_{j=1}^D$. We aim to minimize the empirical risk, see Section 4.2 for details.

Similar to Mansour et al. (2009; 2012) and Hoffman et al. (2018a), we assume that the distribution of the source dataset can be described as a convex combination $\mathbb{P}^s = \sum_{j=1}^D \alpha_j^s \mathbb{P}_j^s$ where $\alpha^s = (\alpha_1^s, \dots, \alpha_D^s)$ is an element of the probability simplex, i.e., $\alpha^s \in \Delta^D := \{\alpha \in \mathbb{R}^D \mid \alpha_j \geq 0 \wedge \sum_{j=1}^D \alpha_j = 1\}$. In other words, α_j^s quantifies the contribution of each

Table 1: Notation

K	number of elementary distributions
M	number of elementary domain bases
N	number of basis vectors
\mathbb{P}^s	combined multi-source distribution
\mathbb{P}_j^s	j -th single-source distribution
\mathbb{P}_j^e	j -th elementary distribution
V_j	j -th domain basis
v_k^j	k -th vector in V_j
α_j^s	coefficient for \mathbb{P}_j^s
α_j^e	coefficient for \mathbb{P}_j^e
β_{ij}	coefficient for sample x_i and μ_{V_j}

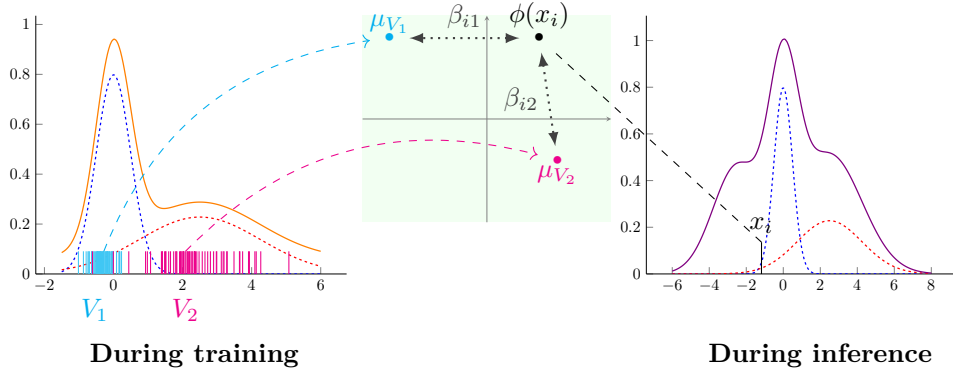


Figure 2: A visualization of an “invariant elementary distribution (I.E.D.)” assumption for domain generalization (DG): both observed and test-time data distributions (orange and violet) are composed of the same set of *unobserved* elementary distributions (blue and red) that remain invariant across different domains. Hence, the first challenge, during training (left panel), is to extract these elementary distributions from the observed data (orange). The unobserved elementary distributions are represented by the elementary bases V_1 and V_2 (cyan and magenta). The second challenge, during inference (right panel), is to create a weighted ensemble of learning machines that utilize the similarities between the embedding of the unseen observation $\phi(x_i)$ and the embeddings of these distributions μ_{V_1} and μ_{V_2} in the RKHS \mathcal{H} (green rectangle) as weights β_{i1} and β_{i2} .

individual source domain to the joint source dataset. For the test domain, prior work Mansour et al. (2009; 2012) and Hoffman et al. (2018a) further makes the important assumption that it lives in the convex hull of the source domains. We aim to tie on these assumptions and connect them to the idea of latent domains, as will discuss in the following paragraph.

For this connection, we express the distribution of each domain as a convex combination of K elementary distributions $\{\mathbb{P}_j^e\}_{j=1}^K \subset \mathcal{P}$, meaning that $\mathbb{P}_j^s = \sum_{j=1}^K \alpha_j^s \mathbb{P}_j^e$ where $\alpha^s \in \Delta^K$. Our main assumption is that these elementary distributions *remain invariant across the domains*. The advantage is that we can find an invariant subspace at a more elementary level as opposed to when we consider the source domains as some sort of basis when generalizing to unseen domains. For a previously unseen distribution, we aim to determine the coefficients α_j^e and quantify the similarity to each elementary domain. Figure 2 illustrates this idea.

Pareto invariance The I.E.D assumption implies the invariant structure in the hypothesis space that can be exploited during training, as shown in the following proposition. The proof is given in Appendix A.1.

Definition 1. Let \mathcal{F} be a hypothesis space of functions and $(R_1, \dots, R_K) : \mathcal{F} \rightarrow \mathbb{R}_+^K$ a vector of risk functionals for $K \geq 2$. Then, the hypothesis $f \in \mathcal{F}$ is said to be Pareto-optimal w.r.t. \mathcal{F} if there exists no $g \in \mathcal{F}$ such that $R_j(g) \geq R_j(f)$ for all $j \in \{1, \dots, K\}$ with $R_j(g) > R_j(f)$ for some j ; see, also, Sener & Koltun (2018, Definition 1).

Proposition 3.1. Let $\mathcal{L} : \mathcal{Y} \times \mathcal{Y} \rightarrow \mathbb{R}_+$ be a non-negative loss function, \mathcal{F} a hypothesis space of functions $f : \mathcal{X} \rightarrow \mathcal{Y}$, and $\mathbb{P}^s(X, Y)$ a data distribution. Suppose the I.E.D assumption holds, i.e., there exist K elementary distributions $\mathbb{P}_1^e, \dots, \mathbb{P}_K^e$ such that $\mathbb{P}^s = \sum_{j=1}^K \alpha_j^s \mathbb{P}_j^e$ for some $\alpha^s \in \Delta^K$. Then, the corresponding Bayes predictor $f^* \in \arg \min_{f \in \mathcal{F}} \mathbb{E}_{(X, Y) \sim \mathbb{P}^s} [\mathcal{L}(Y, f(X))]$ is Pareto-optimal w.r.t. \mathcal{F} and elementary risk functionals (R_1, \dots, R_K) where $R_j(f) := \mathbb{E}_{(X, Y) \sim \mathbb{P}_j^e} [\mathcal{L}(Y, f(X))]$.

Proposition 3.1 implies that, under the I.E.D assumption, Bayes predictors must belong to a subspace of \mathcal{F} called the Pareto set $\mathcal{F}_{\text{Pareto}} \subset \mathcal{F}$ which consists of Pareto-optimal models. In other words, the I.E.D assumption allows us to translate the invariance property of data distributions to the hypothesis space. Since Bayes predictors of *all* future test domains must lie within the Pareto set, which is a strict subset of the original hypothesis space, it is sufficient for the purpose of generalization to maintain only solutions within this Pareto set during the training time. Unfortunately, neither the elementary distributions nor the weights

α are known in practice. Motivated by this theoretical insight, our method presented in Section 4 is designed to uncover them from a multi-source training dataset \mathcal{D}^s .

3.2 Kernel Mean Embedding of Elementary Distributions

We employ the kernel mean embedding (KME) (Berlinet & Thomas-Agnan, 2004; Smola et al., 2007; Muandet et al., 2017) to represent the elementary distributions. Let \mathcal{H} be a reproducing kernel Hilbert space (RKHS) of real-valued functions on \mathcal{X} with a reproducing kernel $k : \mathcal{X} \times \mathcal{X} \rightarrow \mathbb{R}$ (Schölkopf et al., 2001). The KME of a probability measure \mathbb{P} in the \mathcal{H} is defined by $\phi(\mathbb{P}) = \mu_{\mathbb{P}} := \int_{\mathcal{X}} k(\mathbf{x}, \cdot) d\mathbb{P}(\mathbf{x})$. Given I.I.D. samples $\{x_i\}_{i=1}^n$ from \mathbb{P} , $\mu_{\mathbb{P}}$ can be approximated by the empirical KME $\hat{\mu}_{\mathbb{P}} = n^{-1} \sum_{i=1}^n k(x_i, \cdot)$. KME is popular in practice because no explicit distributional assumption, e.g. normality, is required. As such, it has been applied to various machine learning applications, including hypothesis testing (Gretton et al., 2012), training deep generative models (Li et al., 2017), causal inference (Chau et al., 2021), explainability (Chau et al., 2022), and many more.

In this work, we aim to utilise KME to represent our invariant elementary distributions. Moreover, given new test samples, we aim to build a weighted ensemble of predictors from each elementary distributions, where the weights denote similarities between test-time domain and elementary distributions. However, this leads to two challenges, see Figure. 2 for a visualisation.

First, we have no access to samples from the unknown elementary distributions. Thus, the elementary KME cannot be estimated directly from the samples at hand. To this end, we instead seek a proxy KME $\mu_{V_j} := N^{-1} \sum_{k=1}^N k(v_k^j, \cdot)$ for each elementary KME $\mu_{\mathbb{P}_j^e}$ using a domain basis V_j where $V_j = \{v_1^j, \dots, v_N^j\} \subseteq \mathcal{X}$ for each elementary domain $j \in \{1, \dots, M\}$. Hence, the KME μ_{V_j} can be interpreted as the KME of the empirical probability measure $\hat{\mathbb{P}}_{V_j} = N^{-1} \sum_{k=1}^N \delta_{v_k^j}$. Here, we assume that $M = K$ meaning that we approximate all elementary distributions. The sets V_j are referred to as *elementary domain basis*. Intuitively, the elementary domain basis V_1, \dots, V_M represents each elementary distribution by a set of vectors that mimic samples generated from the corresponding distribution.

The second challenge lies in measuring the similarity between samples at test-time and the elementary distributions. We consider two similarity measures utilising their RKHS presentations in the coming section.

With this two challenges tackled, we can proceed to build a convex combination of elementary domain-specific learning machine.

4 Gated Domain Units

This section aims to answer the aforementioned question by instantiating the theoretical ideas presented in Section 3 as a neural network layer consists of a novel gated domain unit (GDU). For the purpose of implementation, let $x \in \mathbb{R}^{h \times w}$ denote the input data point and $h_{\xi} : \mathbb{R}^{h \times w} \rightarrow \mathbb{R}^e$ the feature extractor that transform the input into a representation $\tilde{x} \in \mathbb{R}^e$, e.g. ResNet-50 (He et al., 2016), DenseNet-121 Huang et al. (2017), Graph Isomorphism Networks with virtual nodes (GIN-virtual; Xu et al. (2019) and Gilmer et al. (2017)), DistillBERT Sanh et al. (2020). The final prediction layer is denoted as $g_{\theta} : \mathbb{R}^e \rightarrow \mathcal{Y}$.

GDU consists of three main components:

1. A similarity function $\gamma : \mathcal{H} \times \mathcal{H} \rightarrow \mathbb{R}$ defined on the RKHS that is shared across GDUs.
2. Elementary basis V_j , and
3. learning machine $f(\tilde{x}, \theta_j)$ for each elementary domain $j \in \{1, \dots, M\}$.

In Figure 3, we depict the architecture and how data is processed and information is stored. Given representation \tilde{x}_i , each GDU $_j$ computes the similarity β_{ij} between this sample with their elementary basis V_j using the similarity function γ acting on their RKHS mappings, i.e. $\beta_{ij} = \gamma(\phi(\tilde{x}_i), \mu_{V_j})$. Each GDU is then connected to a learning machine $f(\tilde{x}_i, \theta_j)$ that performs an elementary domain-specific inference. We build the final predictor by taking an ensemble of these learning machines by setting $g_{\theta}(\tilde{x}_i) = \sum_{j=1}^M \beta_{ij} f(\tilde{x}_i, \theta_j)$.

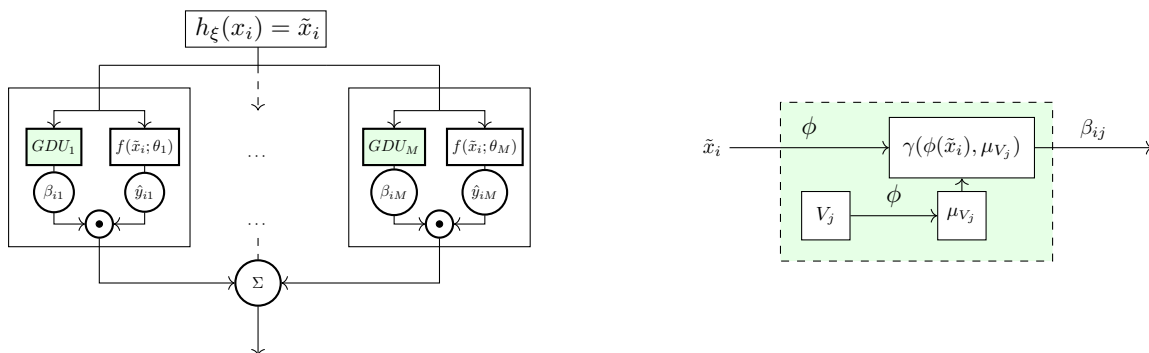


Figure 3: Visualization of the layer (upper panel) and its main component, the GDU (lower panel). The layer consists of multiple GDUs that represent the elementary distributions. During training, the GDUs learn the elementary domain basis V_1, \dots, V_M that approximate these distributions.

In summary, the GDUs leverage the invariant elementary distribution (I.E.D.) assumption and represent our algorithmic contribution. The elementary domain bases $\{V_j\}_j$ are stored as layer weight matrices, thus allowing us to learn them efficiently through backpropagation and avoid the dependency on problem-adaptive methods (e.g., domain-adversarial training) and domain information.

4.1 Choice of Similarity Functions

In this work, we consider two categories of similarity functions γ : one based on distances between inputs and the elementary basis, and the other on projection, akin to kernel sparse coding (Gao et al., 2010; 2013).

4.1.1 Geometry-based Generalization

We consider two geometry-based similarity measure for γ , namely the cosine similarity (CS) (Kim et al., 2019) and maximum mean discrepancy (MMD) (Borgwardt et al., 2006; Gretton et al., 2012). The former considers angles, while the latter considers distances to measure similarity. To ensure $\beta_{ij} := \gamma(\phi(\tilde{x}_i), \mu_{V_j})$ sum up to 1, we apply the kernel softmax function Gao et al. (2019):

$$\beta_{ij} = \gamma(\phi(\tilde{x}_i), \mu_{V_j}) = \frac{\exp(\kappa H(\phi(\tilde{x}_i), \mu_{V_j}))}{\sum_{k=1}^M \exp(\kappa H(\phi(\tilde{x}_i), \mu_{V_k}))},$$

where $\kappa > 0$ is a positive softness parameter for the kernel softmax. For CS, we pick

$$H(\phi(\tilde{x}_i), \mu_{V_j}) = \frac{\langle \phi(\tilde{x}_i), \mu_{V_j} \rangle_{\mathcal{H}}}{\|\phi(\tilde{x}_i)\|_{\mathcal{H}} \|\mu_{V_j}\|_{\mathcal{H}}}$$

while for MMD, we choose

$$H(\phi(\tilde{x}_i), \mu_{V_j}) = -\|\phi(\tilde{x}_i) - \mu_{V_j}\|_{\mathcal{H}}^2$$

instead. When given a batch of samples $\{\tilde{x}_l\}_{l=1}^{n_i}$, we can compute the similarity between the batch with each domain basis by replacing $\phi(\tilde{x}_i)$ with $\tilde{\mu}_i := \frac{1}{n_i} \sum \phi(\tilde{x}_l)$ in the above equations.

4.1.2 Projection-based Generalization

Besides geometry-based similarity, we can also seek for an optimal projection of $\phi(\tilde{x})$ onto the span of $\{\mu_{V_j}\}_{j=1}^M$ such that $\sum_{j=1}^M \|\phi(\tilde{x}_i) - \beta_{ij} \mu_{V_j}\|_{\mathcal{H}}^2$ is small. Note that as the subspace $\mathcal{H}_M := \text{span}\{\mu_{V_j} \mid j = 1, \dots, M\}$ are learnt during training, we could incorporate pairwise orthogonality constraints, i.e. $\langle \mu_{V_j}, \mu_{V_i} \rangle = 0$ for any $i \neq j$, to maximise the ‘‘representation’’ power of this subspace. As a result, this leads to the best possible approximation of the projection of $\phi(\tilde{x}_i)$ onto \mathcal{H} if $\phi(\tilde{x}_i)$ actually lies in the span. See Proposition 4.1.

In practice, given the i^{th} batch of test samples $\{\tilde{x}_l\}_{l=1}^{n_i}$, we could instead find a projection that minimises $\sum_{j=1}^M \|\tilde{\mu}_i - \beta_{ij}\mu_{V_j}\|_{\mathcal{H}}^2$ where $\tilde{\mu}_i$ is the KME of the i^{th} batch.

Proposition 4.1. *Given a distribution \mathbb{P} where $\mu_{\mathbb{P}} \in \text{span}\{\mu_{V_j} \mid j = 1, \dots, M\}$ such that $\langle \mu_{V_j}, \mu_{V_i} \rangle = 0$ for all $i \neq j$. The value of $\sum_{j=1}^M \|\mu_{\mathbb{P}} - \beta_j \mu_{V_j}\|_{\mathcal{H}}^2$ is minimised at $\beta_j^* = \langle \mu_{\mathbb{P}}, \mu_{V_j} \rangle_{\mathcal{H}} / \|\mu_{V_j}\|_{\mathcal{H}}^2$.*

See proof in Appendix A.2). In practice, when given a single sample \tilde{x}_i we could set

$$\beta_{ij} = \frac{\langle \phi(\tilde{x}_i), \mu_{V_j} \rangle}{\|\mu_{V_j}\|_{\mathcal{H}}^2}.$$

If a batch of samples are given instead, we have,

$$\beta_{ij} = \frac{\langle \tilde{\mu}_i, \mu_{V_j} \rangle}{\|\mu_{V_j}\|_{\mathcal{H}}^2}.$$

4.2 Model Training

Following Zhuang et al. (2021), our learning objective function is formalized as $\mathcal{L}(g) + \lambda_D \Omega_D(\|g\|_{\mathcal{H}})$. The goal of the training can be described in terms of the two components of this function. Consider a batch of training data $\{x_1, \dots, x_b\}$, where b is the batch size. During training, we minimize the loss function

$$\mathcal{L}(g) = \frac{1}{b} \sum_{i=1}^b \mathcal{L}(\hat{y}_i, y_i) = \frac{1}{b} \sum_{i=1}^b \mathcal{L}\left(\sum_{j=1}^M \gamma(\phi(\tilde{x}_i), \mu_{V_j}) f_j(\tilde{x}_i), y_i\right)$$

for an underlying task and the respective batch size. In addition, our objective is that the model learns to distinguish between different domains. Thus, the regularization Ω_D is introduced to control the domain basis. In our case, we require the regularization Ω_D to ensure that the KMEs of the elementary domain basis are able to represent the KMEs of the elementary domains. Therefore, we minimize the MMD between the feature mappings $\phi(\tilde{x}_i)$ and the associated representation $\sum_{j=1}^M \beta_{ij} \mu_{V_j}$. Note that $\beta_{ij} = \gamma(\phi(\tilde{x}_i), \mu_{V_j})$. Hence, the regularization $\Omega_D = \Omega_D^{OLS}$ is defined as

$$\Omega_D^{OLS}(\|g\|_{\mathcal{H}}) = \frac{1}{b} \sum_{i=1}^b \|\phi(\tilde{x}_i) - \sum_{j=1}^M \beta_{ij} \mu_{V_j}\|_{\mathcal{H}}^2.$$

The intuition is the objective to represent each feature mapping $\phi(\tilde{x}_i)$ by the domain KMEs μ_{V_j} . Thus, we try to minimize the MMD between the feature map and a combination of μ_{V_j} . The minimum of the stated regularization can be interpreted as the ordinary least square-solution of a regression-problem of $\phi(\tilde{x}_i)$ by the components of \mathcal{H}_M . In other words, we want to ensure that the basis V_j is contained in feature mappings $\phi(\tilde{x}_i)$.

In the particular case of projection, we want the KME of the elementary domain to be orthogonal to ensure high expressive power. For this purpose, the additional term Ω_D^{\perp} will be introduced to ensure the desired orthogonality. Considering a kernel function with $k(x, x) = 1$, orthogonality would require the Gram matrix $K_{ij} = \langle \mu_{V_i}, \mu_{V_j} \rangle_{\mathcal{H}}$ to be close to the identity matrix I . There are a variety of methods for regularizing matrices available (Xie et al., 2017; Bansal et al., 2018). A well-known method to ensure orthogonality is the soft orthogonality regularization $\Omega_D^{\perp} = \lambda \|K - I\|_F^2$ (Bansal et al., 2018). As pointed out by Bansal et al. (2018), since spectral restricted isometry property and mutual coherence regularization can be a promising alternative, we provide an additional implementation for both. Hence, in the case of projection, the regularization is given by

$$\Omega_D(\|g\|_{\mathcal{H}}) = \lambda_{OLS} \Omega_D^{OLS}(\|g\|_{\mathcal{H}}) + \lambda_{ORTH} \Omega_D^{\perp}(\|g\|_{\mathcal{H}}), \quad \lambda_{OLS}, \lambda_{ORTH} \geq 0.$$

Lastly, sparse coding is an efficient technique to find the least possible basis to recover the data subject to a reconstruction error (Olshausen & Field, 1997). Several such applications yield strong performances, for

example in the field of computer vision (Lee et al., 2007; Yang et al., 2009). Kernel sparse coding transfers the reconstruction problem of sparse coding into \mathcal{H} by using the mapping ϕ , and, by applying a kernel function, the reconstruction error is quantified as the inner product (Gao et al., 2010; 2013). To ensure sparsity, we apply the L_1 -norm on the coefficients β and add $\Omega_D^{L_1}(\|\gamma\|) := \|\gamma(\phi(\tilde{x}_i), \mu_{V_j})\|_1$ to the regularization term Ω_D with the corresponding coefficient λ_{L_1} .

5 Experiments

First, we conduct a proof-of-concept study and discuss heuristics for the main parameters. Second, we benchmark our approach based on the standardized WILDS dataset to state-of-the-art DG methods, e.g., CORAL, IRM, and Group DRO. In our experiments, we distinguish two modes of training our layer: (i) **fine tuning**, where we extract features using a pre-trained model, and (ii) **end-to-end training**, where the feature extractor (FE) and the DG layer are jointly trained. Our code for PyTorch and TensorFlow is available on GitHub: <https://github.com/im-ethz/gdu4dg-pytorch> and <https://github.com/im-ethz/pub-gdu4dg>.

5.1 Proof-of-concept based on Digits Classification

Following Feng et al. (2020) among others, we create a multi-source dataset by combining five publicly available digits image datasets, namely MNIST Lecun et al. (1998), MNIST-M Ganin & Lempitsky (2015), SVHN Netzer et al. (2011), USPS, and Synthetic Digits (SYN) Ganin & Lempitsky (2015). Each dataset, except USPS, is split into training and test sets of 25,000 and 9,000 images, respectively. For USPS, we take the whole dataset for the experiment since it contains only 9,298 images. The task is to classify digits between zero and nine. Each of these datasets is considered an out-of-training target domain which is inaccessible during training, and the remaining four are the source domains. Details are given in Appendix B.1.

5.1.1 Parameter selection

From a practical perspective, our layer requires choosing two main hyper-parameters: the number of elementary domains M and since we use the characteristic Gaussian kernel the corresponding parameter σ . The parameter M defines the number of elementary domains and determines the size of the ensemble (i.e., the network size).

Here, we discuss a heuristic to set M . Similar to Matsuura & Harada (2020), we pass the training data through a FE and apply k -means clustering algorithm on the output. Then, we use the Davies-bouldin score to select the optimal number of clusters as the basis to choose M . For example, using MNIST-M as the test domain, cluster scores suggest 10 to 12 clusters (see Figure 4).

As for the parameter σ , we resort to the median heuristic proposed in Muandet et al. (2016) that is $\sigma^2 = \text{median}\{\|\tilde{x}_i - \tilde{x}_j\|^2 : i, j = 1, \dots, n\}$. While both heuristics require a pre-trained FE, cross-validation can act as a reasonable alternative given that we have access to adequate validation data (Koh et al., 2021; Gulrajani & Lopez-Paz, 2020).

5.1.2 DG performance

Although the cluster score has its optimum around 12, we set M to 10 for this experiment considering the additional computational complexity. The hyper-parameters relevant for our layer are summarized in Table 7 in Appendix B.1. In Tale 2, we present the final results for our proof-of-concept experiment. Our method noticeably improves across all tasks the mean accuracy and decreases the standard deviation compared to the ERM and ensemble baselines, making the results more stable across ten iterations.

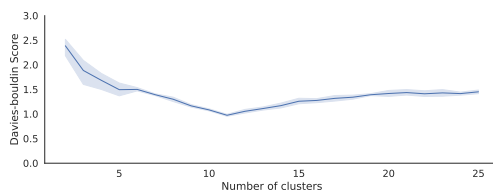


Figure 4: Visualization of the mean and standard deviation of the Davies-bouldin Score across five runs for MNIST-M as the held-out test domain.

Table 2: Results Digits experiment. All experiments were repeated ten times and the mean (standard deviation) accuracy is reported. Best mean results are **bold**.

	MNIST	MNIST-M	SVHN	USPS	SYN
<i>ERM</i>	97.98 (0.34)	63.00 (3.20)	70.18 (2.74)	93.70 (1.74)	83.62 (1.47)
<i>ERM ENSEMBLE</i>	98.21 (0.39)	62.87 (1.50)	72.01 (3.59)	95.16 (0.89)	83.80 (1.22)
FT	CS 98.75 (0.09)	69.44 (0.57)	79.65 (0.89)	96.43 (0.35)	87.94 (0.61)
	MMD 98.74 (0.12)	69.32 (0.46)	79.50 (1.19)	96.54 (0.27)	87.78 (0.6)
	PRO 98.71 (0.11)	69.44 (0.33)	79.4 (1.15)	96.37 (0.36)	87.68 (0.62)
E2E	CS 98.50 (0.09)	67.78 (2.25)	76.76 (1.63)	95.54 (0.45)	87.41 (1.03)
	MMD 98.52 (0.11)	68.80 (0.69)	78.24 (1.09)	95.22 (0.91)	87.78 (0.94)
	PRO 98.13 (0.41)	63.15 (4.32)	75.04 (1.71)	95.49 (0.79)	86.04 (1.27)

5.1.3 Ablation study

First, we discuss the effect of deviating from the cluster heuristic. For this, we vary the corresponding parameter M and analyze the classification performance to validate our heuristic and the sensitivity to the choice of M . The results for the most challenging DG task (MNIST-M) are depicted in Figure 5 (left). In general, the performance difference is slight across the choice of M . However, for FT, we generally observe a higher classification performance than E2E, which also increases with higher M . For FT, we have the highest performance around the heuristically estimated M . In E2E, the performance is slightly lower, and we reach the highest performance when we set M smaller than suggested by the heuristic. This behavior can be explained by the fact that in E2E, the feature extractor and GDUs are jointly trained, and the lower dimensional embedding (i.e., \tilde{x}) is stochastic, which makes learning to approximate the elementary distributions more challenging, especially when their number is high. These results support our heuristic, which we later apply to real-world datasets with a much larger number of source domains.

Lastly, we analyze the sensitivity of the GDUs to the number of elementary domain basis (i.e., N). For this, we vary N and keep the number of elementary domains fixed to the value suggested by the heuristic. We observe that smaller N yields higher results while having the beneficial side-effect of reducing the computational overhead.

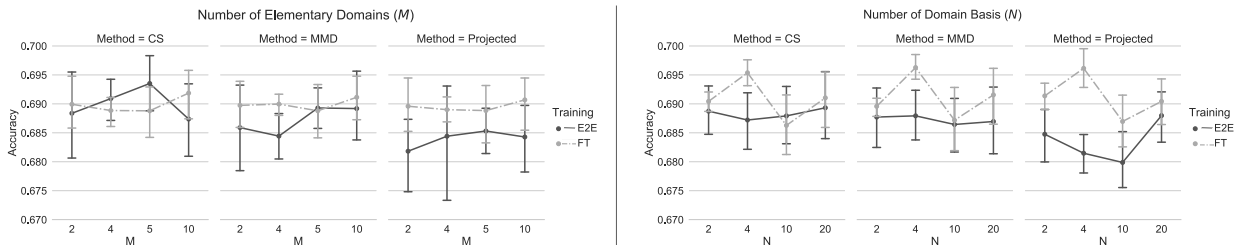


Figure 5: Mean and standard deviation of classification accuracy over 10 runs for varying number of elementary domains (M , left panel) and varying number of vector for each domain basis (N , right panel) for MNIST-M dataset.

The next paragraph focuses on ablating the regularization terms introduced in Section 4), which depends on the form of generalization (i.e., geometry-based or projection-based). For the geometry-based, generalization the regularization is

$$\Omega_D(\|g\|_{\mathcal{H}}) = \lambda_{OLS}\Omega_D^{OLS}(\|g\|_{\mathcal{H}}) + \lambda_{L_1}\Omega_D^{L_1}(\|g\|), \quad (1)$$

where $\lambda_{OLS}, \lambda_{L_1} \geq 0$. In the case of projection, the regularization is given by

$$\Omega_D(\|g\|_{\mathcal{H}}) = \lambda_{OLS}\Omega_D^{OLS}(\|g\|_{\mathcal{H}}) + \lambda_{ORTH}\Omega_D^{\perp}(\|g\|_{\mathcal{H}}) \quad (2)$$

with $\lambda_{OLS}, \lambda_{ORTH} \geq 0$.

We vary in Equation 1 and Equation 2 the corresponding weights λ_1 and λ_2 in the interval of $[0; 0.1]$ and display the mean classification accuracy for the most challenging classification task of MNIST-M in the form of a heatmap. In Figures 6 a-f, we see that the classification accuracy remains on an overall similar level which indicates that our method is not very sensitive to the hyper-parameter change for MNIST-M as the test domain. Nevertheless, we observe that ablating the regularization terms by setting the corresponding weights to zero decreases the classification results and the peaks in performance occur when the regularization is included during training of our method.

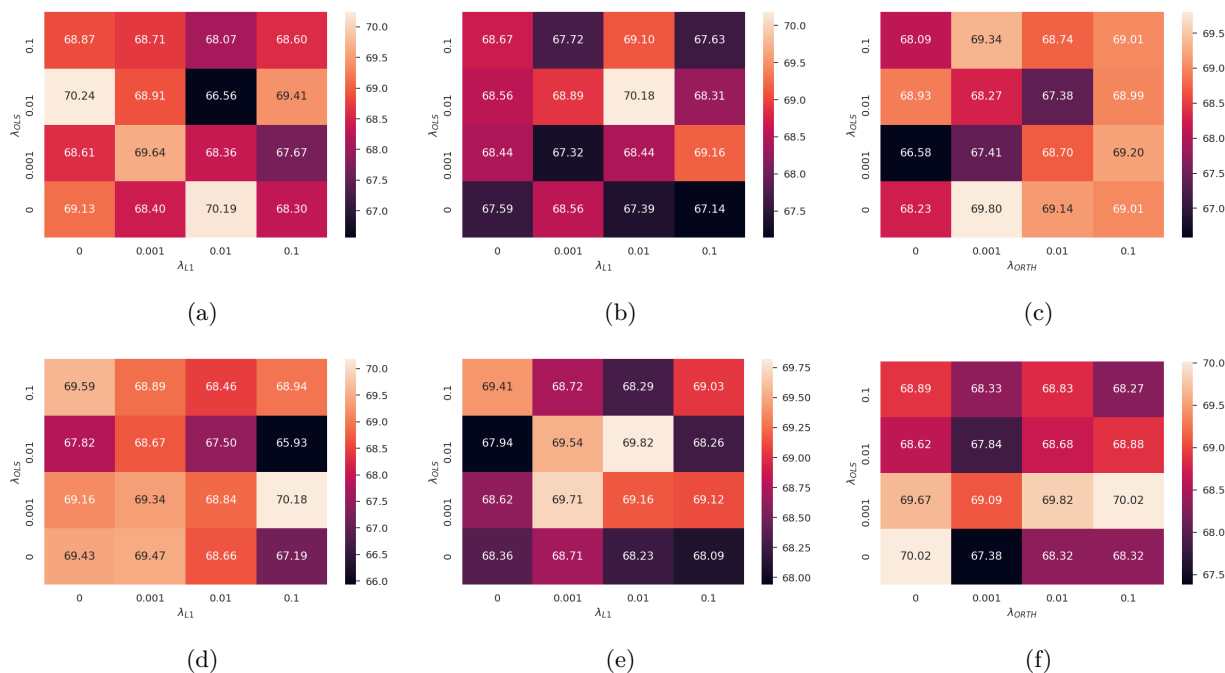


Figure 6: Classification results for varying λ_{L1} and λ_{OLS} in the interval of $[0; 0.1]$ for FT-CS (a), E2E-CS (d), FT-MMD (b) and E2E-MMD (e) and for varying λ_{ORTH} and λ_{OLS} in the interval of $[0; 0.1]$ for FT-Projected (c) and E2E-Projected (f) Projection on MNIST-M.

Applying GDUs comes with additional overhead, especially the regularization that ensures the orthogonality of the elementary domain bases. This additional effort raises a question whether ensuring the theoretical assumptions outweigh the much higher computational effort. Thus, in a second step, we analyze how the orthogonal regularization affects the orthogonality of the elementary domain bases (i.e., spectral restricted isometry property (SRIP) value) and the loss function (i.e., categorical cross-entropy).

In Figure 7, we depict the mean and standard deviation of the spectral restricted isometry property (SRIP) value and loss over five runs for 40 epochs. The SRIP value can be tracked during training with our layer’s callback functionalities. First, we observe that the elementary domains are almost orthogonal when initialized. Training the layer leads in the first epochs to a decrease in orthogonality. This initial decrease happens because cross-entropy has a stronger influence on the optimization than regularization in the first epochs. After five epochs, the cross-entropy decrease to a threshold when the regularization becomes more effective and the orthogonality of the elementary domain bases increases again. In Figure 7, we also observe that ablating the orthogonal regularization, while leading to better orthogonality of the domains, does not significantly affect the overall cross-entropy during training.

This analysis revealed stable results across different sets of hyper-parameters. While the layer is not noticeably sensitive to the choice of regularization strength, we recommend not to omit the regularization completely, although the computational expenses decrease without the orthogonal regularization.

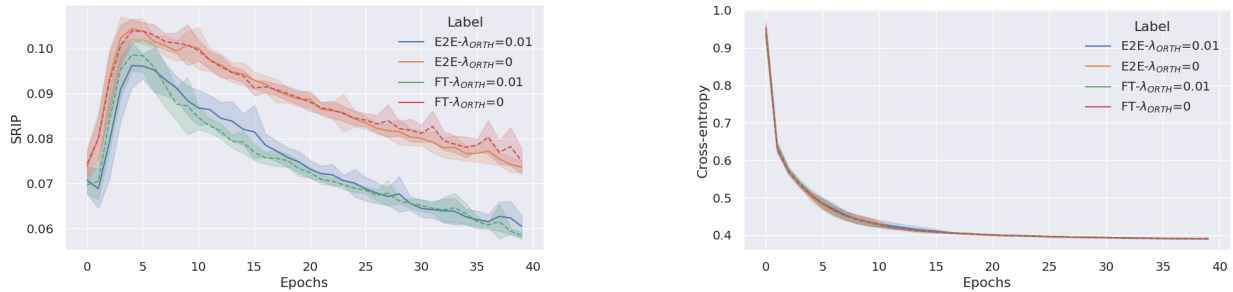


Figure 7: Effect of omitting the orthogonal regularization term $\Omega_D^{\frac{1}{2}}$. Spectral restricted isometry property (SRIP) (left) and categorical cross-entropy (right) with and without orthogonal regularization and their evolution during training for MNSIT-M dataset. The mean and standard deviation presented for End-to-end (E2E) and Fine-tuning (FT) training scenarios are calculated over 10 runs.

Third, in the E2E scenario, the GDUs are jointly trained with the feature extractor. In this particular scenario, we seek to understand how the GDU affect the latent representation learned by the feature extractor. For this, we project the output of the FE trained with a dense layer (ERM) and our layer by t-SNE in Figure 8. The GDU-trained FE yields more concentrated and bounded clusters in comparison to the one trained by ERM. Hence, we observe a positive effect on the FEs representation.

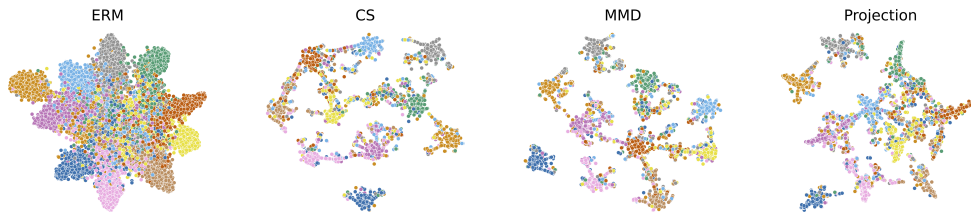


Figure 8: Visualization of t-SNE Embedding on unseen Synthetic Digits Dataset. Colors encode true label.

Lastly, one of the essential questions we seek to answer in this ablation study is on what distributional structure given by the dataset the learned elementary domains learned to represent. Figure 9 depicts the t-SNE embedding of the joint source domains (left), the test, and the elementary domains learned by the GDUs (right). Nine of ten elementary domains form dense clusters around the joint source dataset, indicating that the GDUs learns to represent distributional structures in this multi-source dataset.

5.2 WILDS Benchmark

Currently, two open-source benchmarks are available for a reproducible and rigorous comparison of DG methods, namely DomainBed Gulrajani & Lopez-Paz (2020) and WILDS (Koh et al., 2021). WILDS is a semi-synthetic benchmark that operates under similar assumptions as the source component shift and represents DS occurring under real-world conditions. The advantage in comparison to DomainBed is, that WILDS reveals: Methods that work well on synthetic shifts may drastically fail on real-world shifts such as, for example, invariant risk minimization Gulrajani & Lopez-Paz (2020). To challenge the GDUs under potential model deployment, we chose WILDS.

The following methods reflect the potential and limitations of the research streams followed in DG (see Section 2.1), and thus, serve as our benchmark: CORAL, LISA, IRM, FISH, Group DRO, CGD, and ARM-BN. We closely follow Koh et al. (2021) for the experiments using eight datasets: *Camelyon17*, *FMoW*, *Amazon*, *iWildCam*, and *RxRx1*, *OGB-MolPCBA*, *Civil-Comments*, and *PovertyMap*. Details on datasets and benchmark methods are given in Appendix B.2.

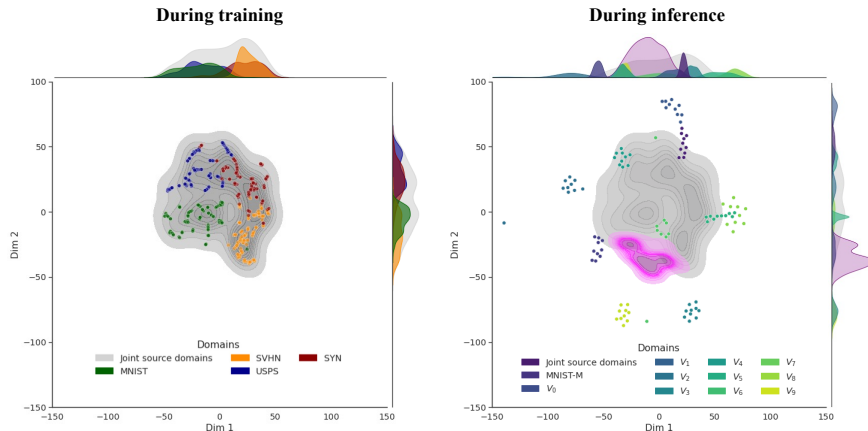


Figure 9: t-SNE visualization of source (left), the elementary and test domains (right). MNIST-M as held-out test domain, FT-MMD. Colors encode source datasets (left) and domain labels (right). Note: Marginals have different scales.

5.2.1 Benchmark results.

To provide a reasonable default parameter for our layer, we apply our heuristic to real-world conditions with a higher number of domains (e.g., 323 camera traps in iWildCam). Figure 10 depicts for each of the eight dataset the cluster score. The scores reach an agreement at $M = 5$, which we set as the default considering the model complexity associated with a higher number.

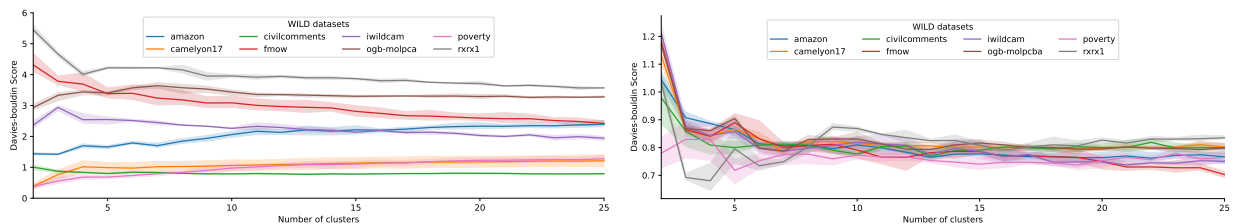


Figure 10: Visualization of the mean and standard deviation of Davies-bouldinn Score for each WILDS dataset. The figure on the left depicts the scores when the output of the FE was clustered with k means, while the figure on the right depicts the scores when the FE output was first embedded with a 2D t-SNE embedding. This embedding yielded better clustering results (i.e., lower Davies-Bouldinn scores).

Table 3 reports the results for $M = 5$. Our approach achieves state-of-the-art OOD performance, however does not outperform the strongest benchmark LISA. Still, the consistent improvement to ERM is a significant advantage compared to the benchmarks since they fall at least once short against ERM (e.g., IRM in RxRx1, Fish in iWildCam, or Coral in OGB-MolPCBA). Thus, our method is especially appealing when domain information is challenging to obtain.

5.2.2 Worst-case vs. average-case performance.

Methods trained to perform well on the worst-case (e.g., underrepresented populations) are prone to a well-known trade-off, thus performing less well on the average cases Eastwood et al. (2022); Rice et al. (2021). Therefore, it is crucial to understand how DG methods are affected by this trade-off. We use the pre-defined average- and wors-case subsets to compute the performance scores and analyse how each method is affected based on the *Poverty*, *FMoW*, and *CivilComments* dataset.

As an example we provide the results for this analysis in Table 4. In general, we observe that this trade-off is apparent also for the benchmarking methods. Of particular note, our method balances this trade-off

Table 3: Benchmarking results. A grey background highlights methods using no domain information for DG. We compute the metrics following Koh et al. (2021) and report the mean (standard deviation). Best benchmark and GDU results are **bold**.

	Camelyon17	FMoW	Amazon	iWildCam	RxRx1	OGB-MolPCBA	Civil Comments	Poverty Map	
No. domains	5	16 x 5	3,920	323	51	120,084	16	23 x 2	
Scores	AVG ACC	WORST-REG ACC	10% ACC	MACRO F1	AVG ACC	AVG WORST-REGION ACC	WORST-GROUP ACC	WORST-U/R R	
ERM	70.3 (6.4)	31.3 (0.17)	53.8 (0.8)	31.0 (1.3)	29.9 (0.4)	27.2 (0.3)	56.0 (3.6)	0.45 (0.06)	
ERM Ensemble	70.0 (9.4)	34.3 (0.18)	54.0 (0.5)	29.5 (0.4)	29.6 (0.3)	26.9 (0.3)	55.6 (0.8)	0.52 (0.08)	
CORAL	59.3 (7.7)	32.8 (0.66)	52.9 (0.8)	32.8 (0.1)	28.4 (0.3)	17.9 (0.5)	65.6 (1.3)	0.44 (0.07)	
Fish	74.7 (7.1)	34.6 (0.18)	53.3 (0.0)	22.0 (1.8)	-	-	75.3 (0.6)	-	
IRM	64.2 (8.1)	32.8 (2.09)	52.4 (0.8)	15.1 (4.9)	8.2 (1.1)	15.6 (0.3)	64.2 (8.1)	0.43 (0.07)	
Group DRO	68.4 (7.3)	31.1 (1.66)	53.3 (0.0)	23.9 (2.1)	22.5 (0.3)	22.4 (0.6)	68.4 (7.3)	0.39 (0.06)	
LISA	77.1 (6.9)	35.5 (0.81)	54.7 (0.0)	-	31.9 (1.0)	-	72.9 (1.0)	-	
CGD	69.4 (7.9)	32.0 (2.26)	-	-	-	-	69.1 (1.9)	0.43 (0.04)	
ARM-BN	-	24.4 (0.54)	-	23.3 (2.8)	31.2 (0.1)	-	-	-	
<i>Ours</i>									
FT	CS	68.5 (8.3)	31.8 (1.2)	54.2 (0.8)	31.2 (0.8)	29.9 (0.3)	27.5 (0.2)	56.0 (3.7)	0.62 (0.13)
	MMD	67.9 (8.0)	31.9 (1.2)	54.2 (0.8)	31.2 (0.8)	29.9 (0.3)	27.5 (0.2)	55.9 (3.7)	0.62 (0.13)
	PRO	66.7 (8.9)	31.8 (1.0)	54.2 (0.8)	30.4 (1.0)	29.8 (0.3)	27.4 (0.2)	56.5 (2.9)	0.62 (0.12)
E2E	CS	66.7 (8.9)	34.0 (1.9)	53.9 (0.7)	27.8 (2.1)	29.7 (0.4)	26.9 (0.1)	55.9 (0.8)	0.46 (0.07)
	MMD	65.7 (6.7)	34.4 (0.7)	54.2 (0.8)	27.4 (1.6)	29.6 (0.2)	27.0 (0.5)	55.8 (0.7)	0.50 (0.06)
	PRO	72.3 (9.5)	32.9 (0.8)	53.8 (0.8)	30.1 (1.2)	29.0 (0.2)	26.6 (0.3)	56.4 (2.1)	0.49 (0.07)

well, achieving improvements in worst- and average-case performance except for *CivilComments*. For this dataset, obtaining domain labels might be the most challenging, yet, using this information seems essential for generalization.

Table 4: Detailed results on the trade-off between worst- and average case performance. A grey background highlights methods using no domain information for DG.

	PovertyMap		CivilComments		FMoW		
	Average-case	Worst-case	Average-case	Worst-case	Average-case	Worst-case	
	PEARSON R	WORST-U/R PEARSON R	AVG ACC	WORST-REGION ACC	AVG ACC	WORST-REGION ACC	
ERM	0.78 (0.04)	0.45 (0.06)	92.1 (0.1)	56.0 (3.6)	52.7 (0.23)	31.3 (0.17)	
ERM Ensemble	0.8 (0.04)	0.52 (0.08)	92.1 (0.0)	55.6 (0.8)	53.6 (0.06)	34.3 (1.85)	
CORAL	0.78 (0.05)	0.44 (0.07)	88.7 (0.5)	65.6 (1.3)	50.1 (0.07)	32.8 (0.66)	
Fish	-	-	89.3 (0.3)	75.3 (0.6)	51.8 (0.32)	34.6 (0.18)	
IRM	0.77 (0.05)	0.43 (0.07)	88.8 (0.7)	66.3 (2.1)	50.4 (0.75)	32.8 (2.09)	
Group DRO	0.75 (0.07)	0.39 (0.06)	89.9 (0.5)	70.0 (2.0)	52.8 (1.15)	31.1 (1.66)	
LISA	-	-	90.1 (0.3)	72.9 (1.0)	52.8 (1.15)	35.5 (0.81)	
CGD	0.77 (0.04)	0.43 (0.04)	89.6 (0.4)	69.1 (1.9)	50.6 (1.39)	32.0 (2.26)	
ARM-BN	-	-	-	-	23.8 (2.0)	72.7 (2.0)	
FT	CS	0.85 (0.04)	0.62 (0.13)	92.3 (0.2)	56.0 (3.7)	53.1 (0.22)	31.8 (1.24)
	MMD	0.85 (0.04)	0.62 (0.13)	92.3 (0.2)	56.0 (3.7)	53.1 (0.22)	31.9 (1.17)
	PRO	0.84 (0.04)	0.62 (0.12)	92.3 (0.3)	56.5 (2.9)	52.7 (0.14)	31.8 (1.08)
E2E	CS	0.78 (0.06)	0.46 (0.07)	92.3 (0.2)	55.9 (0.8)	53.4 (0.25)	34.4 (1.86)
	MMD	0.80 (0.05)	0.50 (0.06)	92.3 (0.2)	55.9 (0.7)	52.7 (0.45)	34.4 (0.71)
	PRO	0.78 (0.04)	0.49 (0.07)	92.2 (0.3)	56.4 (2.1)	52.7 (0.68)	32.9 (0.78)

5.2.3 IID vs. OOD performance.

The relationship between IID and OOD performance can vary, from a positive correlation to a trade-off Wenzel et al. (2022); Teney et al. (2022). Therefore, as a last step, we seek to understand how our method performs on IID data compared to the OOD data, and compare the performance to the benchmarking methods. For this analysis, we leverage the IID and OOD subsets of the *iWildCam* and *RxRx1* experiments.

The IID and OOD performances are presented in Table 5. The trade-off between OOD and IID performance is apparent for some methods (e.g., ARM-BN in *RxRx1*, Coral in *iWildCam*). For *RxRx1*, the GDUs’ OOD performance equals that of ERM; however, we improve in IID performance. For *iWildCam*, we observe a

positive relation between IID and OOD performance. In summary, our modular layer consisting of the GDUs balance the performance on the IID and OOD subsets.

Table 5: Detailed results on the trade-off between IID and OOD performance. A grey background highlights methods using no domain information for DG.

	RxRx1		iWildCam				
	IID	OOD	IID		OOD		
	ACCURACY	ACCURACY	MACRO F1 SCORE	AVG ACC	MACRO F1 SCORE	AVG ACC	
ERM	35.9 (0.4)	29.9 (0.4)	47.1 (1.5)	75.7 (0.4)	30.8 (1.3)	71.5 (2.6)	
ERM Ensemble	35.6 (0.4)	29.9 (0.4)	45.3 (2.1)	74.6 (0.2)	29.5 (0.4)	69.6 (3.2)	
CORAL	34.0 (0.3)	28.4 (0.3)	43.6 (3.3)	73.8 (0.3)	32.7 (0.2)	73.3 (4.3)	
Fish	-	-	40.3 (0.6)	73.8 (0.1)	22.0 (1.8)	64.7 (2.6)	
IRM	9.9 (1.4)	8.2 (1.1)	22.4 (7.7)	59.8 (8.2)	15.1 (4.9)	59.7 (3.8)	
Group DRO	28.1 (0.3)	22.5 (0.3)	37.5 (1.9)	71.6 (2.7)	23.8 (2.0)	72.7 (2.0)	
LISA	41.1 (1.3)	31.9 (1.0)	-	-	-	-	
CGD	-	-	-	-	-	-	
ARM-BN	34.9 (0.2)	31.2 (0.1)	62.0 (4.0)	23.8 (2.0)	72.7 (2.0)	-	
FT	CS	36.0 (0.4)	29.7 (0.4)	47.7 (0.1)	76.6 (0.3)	31.2 (0.8)	72.7 (1.8)
	MMD	36.0 (0.2)	29.6 (0.2)	47.7 (0.1)	76.6 (0.3)	31.2 (0.8)	72.7 (1.8)
	PRO	35.1 (0.3)	29.0 (0.2)	48.2 (0.5)	76.3 (0.4)	30.5 (1.0)	72.5 (1.8)
E2E	CS	36.2 (0.4)	29.9 (0.3)	44.2 (2.0)	74.9 (0.5)	27.8 (2.2)	69.7 (0.3)
	MMD	36.2 (0.4)	29.9 (0.3)	43.4 (1.6)	75.3 (0.2)	27.4 (1.6)	68.3 (2.6)
	PRO	36.0 (0.5)	29.8 (0.3)	45.4 (3.2)	75.0 (1.4)	30.1 (1.3)	71.6 (4.7)

6 Discussion and Conclusion

This work investigated the domain generalization (DG) problem under the I.E.D. assumption: *real-world distributions are composed of elementary distributions that remain invariant across different domains*. We showed its theoretical implications and empirical effectiveness when instantiated in the form of a neural architecture called the GDUs.

Limitations. In contrast to prior work, mostly focusing on aligning training source domains on an observational level given fixed domain labels, our assumption enables modeling the lower-level shifts between them. However, the number of elementary distributions M must be specified in advance by the practitioners. While the application-agnostic heuristic used in our experiments has proven effective, the optimal choice of M remains an open problem. Furthermore, our GDU layer induces additional computational overhead due to the regularization and model size that increases as a function of the number of elementary domains. Noteworthy, our improvement is achieved with a relatively small number of elementary domains indicating that the increased complexity is not a coercive consequence of applying the GDUs. Also, the results achieved are not a consequence of increased complexity, as the ensemble baseline shows.

Outlook. Finally, for the I.E.D. assumption and GDUs to be fully adopted, yielding novel applications that tackle DG in general, it is essential to develop flexible architectures that can efficiently adapt the number of GDUs during training. For example, one could increase M adaptively during training given proper clustering criteria. Following the deterministic annealing formulation Rose (1998), one could split an elementary domain into two once a variance within the domain becomes too large. A generalization of the I.E.D. assumption to situations when some elementary distributions can differ across domains is also an interesting direction to pursue.

References

- Martin Arjovsky, Léon Bottou, Ishaan Gulrajani, and David Lopez-Paz. Invariant risk minimization. 2019. URL <http://arxiv.org/abs/1907.02893>. arxiv:1907.02893.
- Yogesh Balaji, Swami Sankaranarayanan, and Rama Chellappa. MetaReg: Towards domain generalization using meta-regularization. In S. Bengio, H. Wallach, H. Larochelle, K. Grauman, N. Cesa-Bianchi, and R. Garnett (eds.), *Adv. Neural Inf. Process. Syst.*, volume 31. Curran Associates, Inc., 2018.
- P. Bándi, O. Geessink, Q. Manson, M. Van Dijk, M. Balkenhol, M. Hermsen, B. Ehteshami Bejnordi, B. Lee, K. Paeng, A. Zhong, Q. Li, F. G. Zanjani, S. Zinger, K. Fukuta, D. Komura, V. Ovtcharov, S. Cheng, S. Zeng, J. Thagaard, A. B. Dahl, H. Lin, H. Chen, L. Jacobsson, M. Hedlund, M. Çetin, E. Halıcı, H. Jackson, R. Chen, F. Both, J. Franke, H. Küsters-Vandeveld, W. Vreuls, P. Bult, B. van Ginneken, J. van der Laak, and G. Litjens. From Detection of Individual Metastases to Classification of Lymph Node Status at the Patient Level: The CAMELYON17 Challenge. *IEEE Transactions on Medical Imaging*, 38(2):550–560, February 2019. ISSN 1558-254X. doi: 10.1109/TMI.2018.2867350.
- Nitin Bansal, Xiaohan Chen, and Zhangyang Wang. Can we gain more from orthogonality regularizations in training deep networks? In S. Bengio, H. Wallach, H. Larochelle, K. Grauman, N. Cesa-Bianchi, and R. Garnett (eds.), *Adv. Neural Inf. Process. Syst.*, volume 31. Curran Associates, Inc., 2018.
- Shai Ben-David, John Blitzer, Koby Crammer, Alex Kulesza, Fernando Pereira, and Jennifer Wortman Vaughan. A theory of learning from different domains. *Mach. Learn.*, 79(1-2):151–175, 2010. ISSN 15730565. doi: 10/c5bhdk.
- Alain Berlinet and Christine Thomas-Agnan. *Reproducing Kernel Hilbert Spaces in Probability and Statistics*. Kluwer Academic Publishers, 2004.
- Gilles Blanchard, Gyemin Lee, and Clayton Scott. Generalizing from Several Related Classification Tasks to a New Unlabeled Sample. In *Advances in Neural Information Processing Systems*, volume 24, pp. 9, 2011.
- Karsten M Borgwardt, Arthur Gretton, Malte J Rasch, Hans-Peter Kriegel, Bernhard Schölkopf, and Alex J Smola. Integrating structured biological data by Kernel Maximum Mean Discrepancy. *Bioinformatics*, 22(14):e49–e57, July 2006. ISSN 1367-4803. doi: 10/czwvqs.
- Konstantinos Bousmalis, George Trigeorgis, Nathan Silberman, Dilip Krishnan, and Dumitru Erhan. Domain Separation Networks. In D Lee, M Sugiyama, U Luxburg, I Guyon, and R Garnett (eds.), *Adv. Neural Inf. Process. Syst.*, volume 29. Curran Associates, Inc., 2016.
- Siu Lun Chau, Jean-Francois Ton, Javier González, Yee Teh, and Dino Sejdinovic. Bayesimp: Uncertainty quantification for causal data fusion. *Advances in Neural Information Processing Systems*, 34:3466–3477, 2021.
- Siu Lun Chau, Robert Hu, Javier Gonzalez, and Dino Sejdinovic. Rkhs-shap: Shapley values for kernel methods. *Advances in Neural Information Processing Systems*, 35:13050–13063, 2022.
- C. Chen, J. Li, X. Han, X. Liu, and Y. Yu. Compound domain generalization via meta-knowledge encoding. In *2022 IEEE/CVF Conference on Computer Vision and Pattern Recognition (CVPR)*, pp. 7109–7119, Los Alamitos, CA, USA, jun 2022. IEEE Computer Society. doi: 10.1109/CVPR52688.2022.00698. URL <https://doi.ieeecomputersociety.org/10.1109/CVPR52688.2022.00698>.
- Alexander D’Amour, Katherine Heller, Dan Moldovan, Ben Adlam, Babak Alipanahi, Alex Beutel, Christina Chen, Jonathan Deaton, Jacob Eisenstein, Matthew D. Hoffman, Farhad Hormozdiari, Neil Houlsby, Shaobo Hou, Ghassen Jerfel, Alan Karthikesalingam, Mario Lucic, Yian Ma, Cory McLean, Diana Mincu, Akinori Mitani, Andrea Montanari, Zachary Nado, Vivek Natarajan, Christopher Nielson, Thomas F. Osborne, Rajiv Raman, Kim Ramasamy, Rory Sayres, Jessica Schrouff, Martin Seneviratne, Shannon Sequeira, Harini Suresh, Victor Veitch, Max Vladymyrov, Xuezhi Wang, Kellie Webster, Steve Yadlowsky, Taedong Yun, Xiaohua Zhai, and D. Sculley. Underspecification Presents Challenges for Credibility in Modern Machine Learning. November 2020. doi: 2011.03395v2.

-
- Shai Ben David, Tyler Lu, Teresa Luu, and Dávid Pál. Impossibility theorems for domain adaptation. In *Proc. Thirteen. Int. Conf. Artif. Intell. Stat.*, pp. 129–136. JMLR Workshop and Conference Proceedings, 2010.
- Lucas Deecke, Timothy M Hospedales, and Hakan Bilen. Visual representation learning over latent domains. In *International Conference on Learning Representations (ICLR 2022)*, April 2022. URL <https://iclr.cc/>. Tenth International Conference on Learning Representations 2022, ICLR 2022 ; Conference date: 25-04-2022 Through 29-04-2022.
- Cian Eastwood, Alexander Robey, Shashank Singh, Julius von Kügelgen, Hamed Hassani, George J. Pappas, and Bernhard Schölkopf. Probable Domain Generalization via Quantile Risk Minimization. In *Adv. Neural Inf. Process. Syst.*, volume 35. Curran Associates, Inc., October 2022.
- Tongtong Fang, Nan Lu, Gang Niu, and Masashi Sugiyama. Rethinking importance weighting for deep learning under distribution shift. In H. Larochelle, M. Ranzato, R. Hadsell, M. F. Balcan, and H. Lin (eds.), *Adv. Neural Inf. Process. Syst.*, volume 33, pp. 11996–12007. Curran Associates, Inc., 2020.
- Hao-Zhe Feng, Zhaoyang You, Minghao Chen, Tianye Zhang, Minfeng Zhu, Fei Wu, Chao Wu, and Chen Wei. KD3A: Unsupervised Multi-Source Decentralized Domain Adaptation via Knowledge Distillation. *ArXiv Prepr. ArXiv201109757*, 2020. doi: 2011.09757.
- Yaroslav Ganin and Victor Lempitsky. Unsupervised Domain Adaptation by Backpropagation. In Francis Bach and David Blei (eds.), *Proc. 32nd Int. Conf. Mach. Learn.*, volume 37, pp. 1180–1189. PMLR, June 2015.
- Yaroslav Ganin, Evgeniya Ustinova, Hana Ajakan, Pascal Germain, Hugo Larochelle, François Laviolette, Mario Marchand, and Victor Lempitsky. Domain-Adversarial Training of Neural Networks. *Adv. Comput. Vis. Pattern Recognit.*, 17(9783319583464):189–209, May 2015. ISSN 21916594. doi: 10/gjgc2j.
- S. Gao, I. W. Tsang, and L. Chia. Sparse Representation With Kernels. *IEEE Transactions on Image Processing*, 22(2):423–434, February 2013. ISSN 1941-0042. doi: 10/f4nhfq.
- Shenghua Gao, Ivor Wai-Hung Tsang, and Liang-Tien Chia. Kernel Sparse Representation for Image Classification and Face Recognition. In Kostas Daniilidis, Petros Maragos, and Nikos Paragios (eds.), *Comput. Vis. – ECCV 2010*, pp. 1–14, Berlin, Heidelberg, 2010. Springer Berlin Heidelberg. ISBN 978-3-642-15561-1.
- Yingbo Gao, Christian Herold, Weiyue Wang, and Hermann Ney. Exploring Kernel functions in the softmax layer for contextual word classification. *arXiv*, 2019. ISSN 23318422.
- Muhammad Ghifary, W. Bastiaan Kleijn, and Mengjie Zhang. Domain adaptive neural networks for object recognition. *Lect. Notes Comput. Sci. Subser. Lect. Notes Artif. Intell. Lect. Notes Bioinforma.*, 8862: 898–904, 2014. ISSN 16113349. doi: 10/gjgc2m.
- Justin Gilmer, Samuel S. Schoenholz, Patrick F. Riley, Oriol Vinyals, and George E. Dahl. Neural message passing for quantum chemistry. In Doina Precup and Yee Whye Teh (eds.), *Proceedings of the 34th International Conference on Machine Learning*, volume 70 of *Proceedings of Machine Learning Research*, pp. 1263–1272. PMLR, 06–11 Aug 2017. URL <https://proceedings.mlr.press/v70/gilmer17a.html>.
- Boqing Gong, Kristen Grauman, and Fei Sha. Reshaping visual datasets for domain adaptation. In C.J. Burges, L. Bottou, M. Welling, Z. Ghahramani, and K.Q. Weinberger (eds.), *Adv. Neural Inf. Process. Syst.*, volume 26. Curran Associates, Inc., 2013.
- Arthur Gretton, Karsten M. Borgwardt, Malte J. Rasch, Bernhard Schölkopf, and Alexander Smola. A kernel two-sample test. *J. Mach. Learn. Res.*, 13:723–773, 2012. ISSN 15324435.
- Ishaan Gulrajani and David Lopez-Paz. In Search of Lost Domain Generalization. *ArXiv200701434 Cs Stat*, July 2020.

-
- K. He, X. Zhang, S. Ren, and J. Sun. Deep Residual Learning for Image Recognition. In *2016 IEEE Conference on Computer Vision and Pattern Recognition (CVPR)*, pp. 770–778, June 2016. ISBN 1063-6919. doi: 10/gdcfkn.
- C. Hillermeier. Generalized homotopy approach to multiobjective optimization. *Journal of Optimization Theory and Applications*, 110(3):557–583, 2001a.
- C. Hillermeier. *Nonlinear Multiobjective Optimization: A Generalized Homotopy Approach*. International Series of Numerical Mathematics. Springer Basel AG, 2001b.
- Judy Hoffman, Brian Kulis, Trevor Darrell, and Kate Saenko. Discovering Latent Domains for Multisource Domain Adaptation. In Andrew Fitzgibbon, Svetlana Lazebnik, Pietro Perona, Yoichi Sato, and Cordelia Schmid (eds.), *Comput. Vis. – ECCV 2012*, pp. 702–715, Berlin, Heidelberg, 2012. Springer Berlin Heidelberg. ISBN 978-3-642-33709-3.
- Judy Hoffman, Mehryar Mohri, and Ningshan Zhang. Algorithms and theory for multiple-source adaptation. In S. Bengio, H. Wallach, H. Larochelle, K. Grauman, N. Cesa-Bianchi, and R. Garnett (eds.), *Adv. Neural Inf. Process. Syst.*, volume 31. Curran Associates, Inc., 2018a.
- Judy Hoffman, Eric Tzeng, Taesung Park, Jun-Yan Zhu, Phillip Isola, Kate Saenko, Alexei Efros, and Trevor Darrell. CyCADA: Cycle-Consistent Adversarial Domain Adaptation. In Jennifer Dy and Andreas Krause (eds.), *Proc. 35th Int. Conf. Mach. Learn.*, volume 80, pp. 1989–1998, Stockholm, Sweden, 2018b. PMLR.
- Weihua Hu, Gang Niu, Issei Sato, and Masashi Sugiyama. Does distributionally robust supervised learning give robust classifiers? In Jennifer Dy and Andreas Krause (eds.), *Proc. 35th Int. Conf. Mach. Learn.*, volume 80 of *Proceedings of Machine Learning Research*, pp. 2029–2037. PMLR, July 2018.
- Weihua Hu, Matthias Fey, Marinka Zitnik, Yuxiao Dong, Hongyu Ren, Bowen Liu, Michele Catasta, and Jure Leskovec. Open graph benchmark: Datasets for machine learning on graphs, 2021.
- Gao Huang, Zhuang Liu, and Kilian Q. Weinberger. Densely connected convolutional networks. *2017 IEEE Conf. Comput. Vis. Pattern Recognit. CVPR*, pp. 2261–2269, 2017. doi: 10/gfhw3n.
- Geewook Kim, Akifumi Okuno, Kazuki Fukui, and Hidetoshi Shimodaira. Representation learning with weighted inner product for universal approximation of general similarities. In *Proc. Twenty-Eighth Int. Jt. Conf. Artif. Intell. IJCAI-19*, pp. 5031–5038. International Joint Conferences on Artificial Intelligence Organization, July 2019. doi: 10/gjgdb3.
- Taeksoo Kim, Moon-su Cha, Hyunsoo Kim, Jung Kwon Lee, and Jiwon Kim. Learning to Discover Cross-Domain Relations with Generative Adversarial Networks. In Doina Precup and Yee Whye Teh (eds.), *Proc. 34th Int. Conf. Mach. Learn.*, volume 70, pp. 1857–1865, International Convention Centre, Sydney, Australia, 2017. PMLR.
- Pang Wei Koh, Shiori Sagawa, Henrik Marklund, Sang Michael Xie, Marvin Zhang, Akshay Balsubramani, Weihua Hu, Michihiro Yasunaga, Richard Lanus Phillips, Irena Gao, Tony Lee, Etienne David, Ian Stavness, Wei Guo, Berton Earnshaw, Imran Haque, Sara M. Beery, Jure Leskovec, Anshul Kundaje, Emma Pierson, Sergey Levine, Chelsea Finn, and Percy Liang. WILDS: A Benchmark of in-the-Wild Distribution Shifts. In Marina Meila and Tong Zhang (eds.), *Proc. 38th Int. Conf. Mach. Learn.*, volume 139, pp. 5637–5664, Proceedings of Machine Learning Research, 2021. PMLR.
- Daisuke Komura and Shumpei Ishikawa. Machine Learning Methods for Histopathological Image Analysis. *Computational and Structural Biotechnology Journal*, 16:34–42, January 2018. ISSN 2001-0370. doi: 10.1016/j.csbj.2018.01.001.
- Y. Lecun, L. Bottou, Y. Bengio, and P. Haffner. Gradient-based learning applied to document recognition. *Proceedings of the IEEE*, 86(11):2278–2324, November 1998. ISSN 1558-2256. doi: 10/d89c25.

-
- Honglak Lee, Alexis Battle, Rajat Raina, and Andrew Ng. Efficient sparse coding algorithms. In B. Schölkopf, J. Platt, and T. Hoffman (eds.), *Adv. Neural Inf. Process. Syst.*, volume 19. MIT Press, 2007.
- Chun-Liang Li, Wei-Cheng Chang, Yu Cheng, Yiming Yang, and Barnabás Póczos. Mmd gan: Towards deeper understanding of moment matching network. *Advances in neural information processing systems*, 30, 2017.
- Da Li, Yongxin Yang, Yi-Zhe Song, and Timothy M. Hospedales. Learning to generalize: Meta-learning for domain generalization. In *AAAI*, 2018a.
- Haoliang Li, Sinno Jialin Pan, Shiqi Wang, and Alex C. Kot. Domain Generalization with Adversarial Feature Learning. In *2018 IEEE CVF Conf. Comput. Vis. Pattern Recognit.*, pp. 5400–5409, Salt Lake City, UT, June 2018b. IEEE. ISBN 978-1-5386-6420-9. doi: 10/ghv245.
- Haoliang Li, Wen Li, and Shiqi Wang. Discovering and incorporating latent target-domains for domain adaptation. *Pattern Recognition*, 108:107536, December 2020. ISSN 0031-3203. doi: 10.1016/j.patcog.2020.107536.
- Ya Li, Xinmei Tian, Mingming Gong, Yajing Liu, Tongliang Liu, Kun Zhang, and Dacheng Tao. Deep Domain Generalization via Conditional Invariant Adversarial Networks. In Vittorio Ferrari, Martial Hebert, Cristian Sminchisescu, and Yair Weiss (eds.), *Comput. Vis. – ECCV 2018*, pp. 647–663, Cham, 2018c. Springer International Publishing. ISBN 978-3-030-01267-0.
- Yiyang Li, Yongxin Yang, Wei Zhou, and Timothy Hospedales. Feature-critic networks for heterogeneous domain generalization. In Kamalika Chaudhuri and Ruslan Salakhutdinov (eds.), *Proc. 36th Int. Conf. Mach. Learn.*, volume 97 of *Proceedings of Machine Learning Research*, pp. 3915–3924. PMLR, June 2019.
- Ming-Yu Liu and Oncel Tuzel. Coupled Generative Adversarial Networks. In D Lee, M Sugiyama, U Luxburg, I Guyon, and R Garnett (eds.), *Adv. Neural Inf. Process. Syst.*, volume 29. Curran Associates, Inc., 2016.
- Mingsheng Long, Yue Cao, Jianmin Wang, and Michael I. Jordan. Learning transferable features with deep adaptation networks. *32nd Int. Conf. Mach. Learn. ICML 2015*, 1:97–105, 2015.
- Mingsheng Long, ZHANGJIE CAO, Jianmin Wang, and Michael I Jordan. Conditional adversarial domain adaptation. In S. Bengio, H. Wallach, H. Larochelle, K. Grauman, N. Cesa-Bianchi, and R. Garnett (eds.), *Adv. Neural Inf. Process. Syst.*, volume 31. Curran Associates, Inc., 2018.
- Pingchuan Ma, Tao Du, and Wojciech Matusik. Efficient continuous pareto exploration in multi-task learning. In *Proceedings of the 37th International Conference on Machine Learning*. JMLR.org, 2020.
- Yishay Mansour, Mehryar Mohri, and Afshin Rostamizadeh. Domain adaptation with multiple sources. In D. Koller, D. Schuurmans, Y. Bengio, and L. Bottou (eds.), *Adv. Neural Inf. Process. Syst.*, volume 21. Curran Associates, Inc., 2009.
- Yishay Mansour, Mehryar Mohri, and Afshin Rostamizadeh. Multiple Source Adaptation and the Renyi Divergence. *Proc. 25th Conf. Uncertain. Artif. Intell. UAI 2009*, pp. 367–374, May 2012.
- Toshihiko Matsuura and Tatsuya Harada. Domain Generalization Using a Mixture of Multiple Latent Domains. *AAAI*, 34(07):11749–11756, April 2020. doi: 10.1609/aaai.v34i07.6846.
- Joao Monteiro, Xavier Gibert, Jianqiao Feng, Vincent Dumoulin, and Dar-Shyang Lee. Domain Conditional Predictors for Domain Adaptation. In Luca Bertinetto, João F. Henriques, Samuel Albanie, Michela Paganini, and Gül Varol (eds.), *NeurIPS 2020 Workshop Pre-Regist. Mach. Learn.*, volume 148, pp. 193–220, Proceedings of Machine Learning Research, 2021. PMLR.
- Krikamol Muandet, David Balduzzi, and Bernhard Schölkopf. Domain Generalization via Invariant Feature Representation. In Sanjoy Dasgupta and David McAllester (eds.), *Proc. 30th Int. Conf. Mach. Learn.*, pp. 10–18. PMLR, February 2013.

-
- Krikamol Muandet, Kenji Fukumizu, Bharath Sriperumbudur, and Bernhard Schölkopf. *Kernel Mean Embedding of Distributions: A Review and Beyond*, volume 10. May 2016.
- Krikamol Muandet, Kenji Fukumizu, Bharath Sriperumbudur, and Bernhard Schölkopf. Kernel mean embedding of distributions: A review and beyond. *Foundations and Trends in Machine Learning*, 10(1-2): 1–141, 2017.
- Yuval Netzer, Tao Wang, Adam Coates, Alessandro Bissacco, Bo Wu, and Andrew Y. Ng. Reading digits in natural images with unsupervised feature learning. In *NIPS Workshop Deep Learn. Unsupervised Feature Learn. 2011*, 2011.
- Bruno A. Olshausen and David J. Field. Sparse coding with an overcomplete basis set: A strategy employed by V1? *Vision Res.*, 37(23):3311–3325, 1997. ISSN 0042-6989. doi: 10/dn4knd.
- X. Peng and K. Saenko. Synthetic to Real Adaptation with Generative Correlation Alignment Networks. In *2018 IEEE Winter Conference on Applications of Computer Vision (WACV)*, pp. 1982–1991, March 2018. doi: 10/gjgc2k.
- X. Peng, Q. Bai, X. Xia, Z. Huang, K. Saenko, and B. Wang. Moment Matching for Multi-Source Domain Adaptation. In *2019 IEEE/CVF International Conference on Computer Vision (ICCV)*, pp. 1406–1415, 2019. ISBN 2380-7504. doi: 10/ghfhmt.
- Jonas Peters, Peter Bühlmann, and Nicolai Meinshausen. Causal inference by using invariant prediction: identification and confidence intervals. *Journal of the Royal Statistical Society: Series B (Statistical Methodology)*, 78(5):947–1012, 2016.
- Vihari Piratla, Praneeth Netrapalli, and Sunita Sarawagi. Efficient Domain Generalization via Common-Specific Low-Rank Decomposition. In Hal Daumé III and Aarti Singh (eds.), *Proc. 37th Int. Conf. Mach. Learn.*, volume 119, pp. 7728–7738, Proceedings of Machine Learning Research, 2020. PMLR.
- Vihari Piratla, Praneeth Netrapalli, and Sunita Sarawagi. Focus on the Common Good: Group Distributional Robustness Follows, April 2022.
- J. Quinero-Candela, M. Sugiyama, A. Schwaighofer, and N.D. Lawrence. *Dataset Shift in Machine Learning*. Neural Information Processing Series. MIT Press, 2022. ISBN 978-0-262-54587-7.
- Jie Ren, Peter J. Liu, Emily Fertig, Jasper Snoek, Ryan Poplin, Mark Depristo, Joshua Dillon, and Balaji Lakshminarayanan. Likelihood ratios for out-of-distribution detection. In H. Wallach, H. Larochelle, A. Beygelzimer, F. dAlché-Buc, E. Fox, and R. Garnett (eds.), *Adv. Neural Inf. Process. Syst.*, volume 32. Curran Associates, Inc., 2019.
- Leslie Rice, Anna Bair, Huan Zhang, and J. Zico Kolter. Robustness between the worst and average case. In M. Ranzato, A. Beygelzimer, Y. Dauphin, P.S. Liang, and J. Wortman Vaughan (eds.), *Adv. Neural Inf. Process. Syst.*, volume 34, pp. 27840–27851. Curran Associates, Inc., 2021.
- K. Rose. Deterministic annealing for clustering, compression, classification, regression, and related optimization problems. *Proceedings of the IEEE*, 86(11):2210–2239, 1998. doi: 10.1109/5.726788.
- Shiori Sagawa, Pang Wei Koh, Tatsunori B Hashimoto, and Percy Liang. Distributionally Robust Neural Networks for Group Shifts: On the Importance of Regularization for Worst-Case Generalization. In *International Conference on Learning Representations 2020*, pp. 19, 2020.
- Victor Sanh, Lysandre Debut, Julien Chaumond, and Thomas Wolf. Distilbert, a distilled version of bert: smaller, faster, cheaper and lighter, 2020.
- Bernhard Schölkopf. Causality for Machine Learning. *arXiv*, pp. 1–20, 2019. ISSN 23318422.
- Bernhard Schölkopf, Ralf Herbrich, and Alex J. Smola. A Generalized Representer Theorem. In G. Goos, J. Hartmanis, J. van Leeuwen, David Helmbold, and Bob Williamson (eds.), *Computational Learning Theory*, volume 2111, pp. 416–426. Springer Berlin Heidelberg, Berlin, Heidelberg, 2001. ISBN 978-3-540-42343-0 978-3-540-44581-4. doi: 10.1007/3-540-44581-1_27.

-
- Bernhard Schölkopf, Francesco Locatello, Stefan Bauer, Nan Rosemary Ke, Nal Kalchbrenner, Anirudh Goyal, and Yoshua Bengio. Toward causal representation learning. *Proceedings of the IEEE*, 109(5):612–634, 2021.
- Ozan Sener and Vladlen Koltun. Multi-task learning as multi-objective optimization. In *Proceedings of the 32nd International Conference on Neural Information Processing Systems*, pp. 525–536, Red Hook, NY, USA, 2018. Curran Associates Inc.
- Yuge Shi, Jeffrey Seely, Philip H. S. Torr, N. Siddharth, Awni Hannun, Nicolas Usunier, and Gabriel Synnaeve. Gradient Matching for Domain Generalization. *arXiv*, 2021. doi: 2104.09937.
- Alexander J. Smola, Arthur Gretton, Le Song, and Bernhard Schölkopf. A Hilbert space embedding for distributions. In *Proceedings of the 18th International Conference on Algorithmic Learning Theory (ALT)*, pp. 13–31. Springer-Verlag, 2007.
- Masashi Sugiyama and Motoaki Kawanabe. *Machine Learning in Non-Stationary Environments: Introduction to Covariate Shift Adaptation*. The MIT Press, March 2012. ISBN 978-0-262-01709-1.
- Baochen Sun, Jiashi Feng, and Kate Saenko. Return of frustratingly easy domain adaptation. *30th AAAI Conf. Artif. Intell. AAAI 2016*, (Figure 1):2058–2065, 2016.
- Rohan Taori, Achal Dave, Vaishaal Shankar, Nicholas Carlini, Benjamin Recht, and Ludwig Schmidt. Measuring Robustness to Natural Distribution Shifts in Image Classification. *arXiv:2007.00644*, September 2020.
- David Tellez, Geert Litjens, Péter Bándi, Wouter Bulten, John-Melle Bokhorst, Francesco Ciompi, and Jeroen van der Laak. Quantifying the effects of data augmentation and stain color normalization in convolutional neural networks for computational pathology. *Medical Image Analysis*, 58:101544, December 2019. ISSN 1361-8415. doi: 10.1016/j.media.2019.101544.
- Damien Teney, Yong Lin, Seong Joon Oh, and Ehsan Abbasnejad. ID and OOD Performance Are Sometimes Inversely Correlated on Real-world Datasets, September 2022.
- E. Tzeng, J. Hoffman, K. Saenko, and T. Darrell. Adversarial Discriminative Domain Adaptation. In *2017 IEEE Conference on Computer Vision and Pattern Recognition (CVPR)*, pp. 2962–2971, July 2017. ISBN 1063-6919. doi: 10/gf5br3.
- Eric Tzeng, Judy Hoffman, Ning Zhang, Kate Saenko, and Trevor Darrell. Deep Domain Confusion: Maximizing for Domain Invariance. January 2014.
- Vladimir N. Vapnik. *Statistical Learning Theory*. Wiley-Interscience, 1998.
- Mitko Veta, Paul J. van Diest, Mehdi Jiwa, Shaimaa Al-Janabi, and Josien P. W. Pluim. Mitosis Counting in Breast Cancer: Object-Level Interobserver Agreement and Comparison to an Automatic Method. *PLOS ONE*, 11(8):e0161286, August 2016. doi: 10.1371/journal.pone.0161286.
- Jindong Wang, Cuiling Lan, Chang Liu, Yidong Ouyang, and Tao Qin. Generalizing to unseen domains: A survey on domain generalization. *CoRR*, abs/2103.03097, 2021. URL <https://arxiv.org/abs/2103.03097>.
- Florian Wenzel, Andrea Dittadi, Peter Vincent Gehler, Carl-Johann Simon-Gabriel, Max Horn, Dominik Zietlow, David Kernert, Chris Russell, Thomas Brox, Bernt Schiele, Bernhard Schölkopf, and Francesco Locatello. Assaying Out-Of-Distribution Generalization in Transfer Learning. In *Adv. Neural Inf. Process. Syst. 22*. Curran Associates, Inc., October 2022.
- Pengtao Xie, B. Póczos, and E. Xing. Near-orthogonality regularization in kernel methods. In *UAI*, 2017.
- Keyulu Xu, Weihua Hu, Jure Leskovec, and Stefanie Jegelka. How powerful are graph neural networks? In *International Conference on Learning Representations*, 2019. URL <https://openreview.net/forum?id=ryGs6iA5Km>.

-
- Jianchao Yang, Kai Yu, Yihong Gong, and Thomas Huang. Linear spatial pyramid matching using sparse coding for image classification. In *2009 IEEE Conf. Comput. Vis. Pattern Recognit.*, pp. 1794–1801, 2009. doi: 10/d52z9q.
- Huaxiu Yao, Yu Wang, Sai Li, Linjun Zhang, Weixin Liang, James Zou, and Chelsea Finn. Improving Out-of-Distribution Robustness via Selective Augmentation, June 2022.
- Z. Yi, H. Zhang, P. Tan, and M. Gong. DualGAN: Unsupervised Dual Learning for Image-to-Image Translation. In *2017 IEEE International Conference on Computer Vision (ICCV)*, pp. 2868–2876, 2017. ISBN 2380-7504. doi: 10/ggv876.
- Kun Zhang, Mingming Gong, Petar Stojanov, Biwei Huang, QINGSONG LIU, and Clark Glymour. Domain adaptation as a problem of inference on graphical models. In H. Larochelle, M. Ranzato, R. Hadsell, M. F. Balcan, and H. Lin (eds.), *Adv. Neural Inf. Process. Syst.*, volume 33, pp. 4965–4976. Curran Associates, Inc., 2020.
- Marvin Zhang, Henrik Marklund, Nikita Dhawan, Abhishek Gupta, Sergey Levine, and Chelsea Finn. Adaptive risk minimization: Learning to adapt to domain shift. In M. Ranzato, A. Beygelzimer, Y. Dauphin, P.S. Liang, and J. Wortman Vaughan (eds.), *Adv. Neural Inf. Process. Syst.*, volume 34, pp. 23664–23678. Curran Associates, Inc., 2021.
- Han Zhao, Shanghang Zhang, Guanhang Wu, José M F Moura, Joao P Costeira, and Geoffrey J Gordon. Adversarial Multiple Source Domain Adaptation. In S Bengio, H Wallach, H Larochelle, K Grauman, N Cesa-Bianchi, and R Garnett (eds.), *Adv. Neural Inf. Process. Syst.*, volume 31. Curran Associates, Inc., 2018.
- S. Zhao, X. Yue, S. Zhang, B. Li, H. Zhao, B. Wu, R. Krishna, J. E. Gonzalez, A. L. Sangiovanni-Vincentelli, S. A. Seshia, and K. Keutzer. A Review of Single-Source Deep Unsupervised Visual Domain Adaptation. *IEEE Transactions on Neural Networks and Learning Systems*, pp. 1–21, 2020. ISSN 2162-2388. doi: 10/ghtz3h.
- Kaiyang Zhou, Yongxin Yang, Timothy Hospedales, and Tao Xiang. Deep Domain-Adversarial Image Generation for Domain Generalisation. *AAAI*, 34(07):13025–13032, April 2020. doi: 10/gj4mr2.
- Kaiyang Zhou, Ziwei Liu, Yu Qiao, Tao Xiang, and Chen Change Loy. Domain Generalization: A Survey. *ArXiv210302503 Cs*, March 2021a.
- Kaiyang Zhou, Yongxin Yang, Yu Qiao, and Tao Xiang. Domain Generalization with MixStyle. In *International Conference on Learning Representations*, pp. 15, 2021b.
- J. Zhu, T. Park, P. Isola, and A. A. Efros. Unpaired Image-to-Image Translation Using Cycle-Consistent Adversarial Networks. In *2017 IEEE International Conference on Computer Vision (ICCV)*, pp. 2242–2251, 2017. ISBN 2380-7504. doi: 10/gfhw33.
- F. Zhuang, Z. Qi, K. Duan, D. Xi, Y. Zhu, H. Zhu, H. Xiong, and Q. He. A Comprehensive Survey on Transfer Learning. *Proceedings of the IEEE*, 109(1):43–76, January 2021. ISSN 1558-2256. doi: 10/ghcsqr.

A Proofs

A.1 Proof of Proposition 3.1

Proof. The result holds trivially for $K = 1$. For $K \geq 2$ and by the I.E.D assumption, $\mathbb{P}^s(X, Y) = \sum_{j=1}^K \alpha_j \mathbb{P}_j(X, Y)$ for some $\alpha \in \Delta^K$. Then, we can write the risk functional for each $f \in \mathcal{F}$ as $R(f) = \int \mathcal{L}(y, f(x)) d\mathbb{P}^s(x, y) = \int \mathcal{L}(y, f(x)) d(\sum_{j=1}^K \alpha_j \mathbb{P}_j(x, y)) = \sum_{j=1}^K \alpha_j \int \mathcal{L}(y, f(x)) d\mathbb{P}_j(x, y) = \sum_{j=1}^K \alpha_j R_j(f)$ where $R_j : \mathcal{F} \rightarrow \mathbb{R}_+$ is the elementary risk functional associated with the elementary distribution $\mathbb{P}_j(X, Y)$. Hence, the Bayes predictors satisfy

$$f^* \in \arg \min_{f \in \mathcal{F}} R(f) = \arg \min_{f \in \mathcal{F}} \sum_{j=1}^K \alpha_j R_j(f). \quad (\text{A.3})$$

Since the rhs of equation A.3 corresponds to the linear scalarization of a multi-objective function (R_1, \dots, R_K) , its solution (i.e., a stationary point) is Pareto-optimal with respect to these objective functions (Ma et al., 2020, Definition 3.1); see, also, (Hillermeier, 2001a;b). That is, the Bayes predictors for the data distribution that satisfies the I.E.D assumption must belong to the Pareto set $\mathcal{F}_{\text{Pareto}} := \{f^* : f^* = \arg \min_{f \in \mathcal{F}} \sum_{j=1}^K \alpha_j R_j(f), \alpha \in \Delta^K\} \subset \mathcal{F}$. \square

A.2 Proof of Proposition 4.1

Proof. Suppose we have a representation,

$$\mu_{\mathbb{P}} = \sum_{j=1}^M \beta_j \mu_{V_j} \quad \langle \mu_{V_i}, \mu_{V_i} \rangle_{\mathcal{H}} = 0 \quad \forall i \neq j, \quad (\text{A.1})$$

i.e. $\{\mu_{V_1}, \dots, \mu_{V_m}\}$ are pairwise orthogonal. We want to minimize the MMD by minimizing

$$\|\mu_{\mathbb{P}} - \sum_{j=1}^M \beta_j \mu_{V_j}\|_{\mathcal{H}}^2 = \underbrace{\langle \mu_{\mathbb{P}}, \mu_{\mathbb{P}} \rangle_{\mathcal{H}}}_{\|\mu_{\mathbb{P}}\|_{\mathcal{H}}^2} - 2 \langle \mu_{\mathbb{P}}, \sum_{j=1}^M \beta_j \mu_{V_j} \rangle_{\mathcal{H}} + \langle \sum_{i=1}^M \beta_i \mu_{V_i}, \sum_{j=1}^M \beta_j \mu_{V_j} \rangle_{\mathcal{H}} \quad (\text{A.2})$$

$$= \|\mu_{\mathbb{P}}\|_{\mathcal{H}}^2 - 2 \sum_{j=1}^M \beta_j \langle \mu_{\mathbb{P}}, \mu_{V_j} \rangle_{\mathcal{H}} + \sum_{i=1}^M \sum_{j=1}^M \beta_i \beta_j \underbrace{\langle \mu_{V_i}, \mu_{V_j} \rangle_{\mathcal{H}}}_{\delta_{ij} \langle \mu_{V_i}, \mu_{V_j} \rangle_{\mathcal{H}}} \quad (\text{A.3})$$

$$= \|\mu_{\mathbb{P}}\|_{\mathcal{H}}^2 - 2 \sum_{j=1}^M \beta_j \langle \mu_{\mathbb{P}}, \mu_{V_j} \rangle_{\mathcal{H}} + \sum_{j=1}^M \beta_j^2 \|\mu_{V_j}\|_{\mathcal{H}}^2. \quad (\text{A.4})$$

By defining

$$\Phi(\beta) := \|\mu_{\mathbb{P}} - \sum_{j=1}^M \beta_j \mu_{V_j}\|_{\mathcal{H}}^2, \quad (\text{A.5})$$

we can simply find the optimal β_j by using the partial derivative

$$\frac{\partial \Phi}{\partial \beta_j} = -2 \langle \mu_{\mathbb{P}}, \mu_{V_j} \rangle_{\mathcal{H}} + 2 \beta_j \|\mu_{V_j}\|_{\mathcal{H}}^2 \stackrel{!}{=} 0 \quad (\text{A.4})$$

$$\Leftrightarrow \beta_j \|\mu_{V_j}\|_{\mathcal{H}}^2 = \langle \mu_{\mathbb{P}}, \mu_{V_j} \rangle_{\mathcal{H}} \quad (\text{A.5})$$

$$\Leftrightarrow \beta_j^* = \frac{\langle \mu_{\mathbb{P}}, \mu_{V_j} \rangle_{\mathcal{H}}}{\|\mu_{V_j}\|_{\mathcal{H}}^2}. \quad (\text{A.6})$$

Please note that the function Φ is convex. \square

B Experiments

In this section, we provide a detailed description of the DG experiment presented in Section 5. Our Digits experiments are implemented using TensorFlow 2.4.1 and TensorFlow Probability 0.12.1. For the WILDS benchmarking we use our PyTorch (version 1.11.0). All source code will be made available on GitHub <https://github.com/> (TensorFlow) and <https://github.com/> (PyTorch).

For the Gated Domain layer, we considered two modes of model training: fine tuning (FT) and end-to-end training (E2E). In FT scenario, we first pre-train the FE in the ERM single fashion. Then, we extract features using the pre-trained model and pass them to the Gated Domain layer for training the latter. For the E2E training, however, the whole model including the FE and Gated Domain layer is trained jointly from the very beginning.

B.1 Digits Experiment

Our experiment setup is closely related to Peng et al. (2019); Feng et al. (2020); Zhang et al. (2020); Zhao et al. (2018). We used the digits data from <https://github.com/FengHZ/KD3A> [last accessed on 2022-05-17, available under MIT License.] published in Feng et al. (2020). Our experimental setup regarding datasets, data loader, and FE are based on existing work (Feng et al., 2020; Peng et al., 2019). The structure of the FE is summarized in Table 6 and the subsequent learning machine is a dense layer.

In the Empirical Risk Minimization (ERM) single experiment, we add a dense layer with 10 outputs (activation= \tanh) as a classifier to the FE. In the Empirical Risk Minimization (ERM) ensemble experiment, we add M classification heads (a dense layers with 10 outputs and \tanh activation each) to the FE and average their output for the final prediction. This sets a baseline for our Gated Domain layer to show performance gain against the ERM model with the same number of learning machines.

For training, we resorted to the Adam optimizer with a learning rate of 0.001. We used early stopping and selected the best model weights according to the validation accuracy. For the validation data, we used the combined test splits only of the respective source datasets. The batch size was set to 512. Although the Gated Domain layer requires more computation resources than the ERM models, all digits experiments were conducted on a single GPU (NVIDIA GeForce RTX 3090).

Table 7: Parameters for Gated Domain layer in Digits and Digit-DG Experiments for the Fine Tuning (FT) and End-to-end training (E2E) Settings. In case of Projection, we chose the spectral restricted isometry property (SRIP) as the orthogonal regularization Ω_D^\perp . In the FT setting, we applied the median heuristics presented above to estimate σ of the Gaussian kernel function, where the estimator is denoted as $\hat{\sigma}$. Since median heuristic is not applicable for the E2E scenario, σ was fixed to 7.5 for E2E.

Table 6: Feature Extractor used for the Digits Experiment

FEATURE EXTRACTOR	
LAYER TYPE	OUTPUT SHAPE
2D-CONVOLUTIONAL LAYER	(32, 32, 64)
BATCH NORMALIZATION	(32, 32, 64)
MAXPOOLING 2D	(16, 16, 64)
2D-CONVOLUTIONAL LAYER	(16, 16, 64)
BATCH NORMALIZATION	(16, 16, 64)
MAXPOOLING 2D	(8, 8, 64)
2D-CONVOLUTIONAL LAYER	(8, 8, 128)
BATCH NORMALIZATION	(8, 8, 128)
MAXPOOLING 2D	(4, 4, 128)
FLATTEN	(2048)
DENSE LAYER	(3072)
BATCH NORMALIZATION	(3072)
DROPOUT	(3072)
BATCH NORMALIZATION	(2048)
DENSE LAYER	(2048)

EXPERIMENT		M	N	λ_{L_1}	λ_{OLS}	λ_{ORTH}	σ	κ
FT	CS	5	10	$1e^{-3}$	$1e^{-3}$	-	$\hat{\sigma}$	2
	MMD	5	10	$1e^{-3}$	$1e^{-3}$	-	$\hat{\sigma}$	2
	PROJECTION	5	10	$1e^{-3}$	$1e^{-3}$	$1e^{-8}$	$\hat{\sigma}$	-
E2E	CS	5	10	$1e^{-3}$	$1e^{-3}$	-	7.5	2
	MMD	5	10	$1e^{-3}$	$1e^{-3}$	-	7.5	2
	PROJECTION	5	10	$1e^{-3}$	$1e^{-3}$	$1e^{-8}$	7.5	-

B.2 WILDS Benchmarking Experiments

For comparison of our approach and benchmarking, we followed the standard procedure of WILDS experiments, described in Koh et al. (2021). As a technical note, all WILDS experiments have been implemented in Pytorch (version $\geq 1.7.0$) based on the specifications made in Koh et al. (2021) and their code published on <https://github.com/p-lambda/wilds> [last accessed on 2022-05-17, available under MIT License]. The results for the benchmarks were retrieved from the official leaderboard <https://wilds.stanford.edu/leaderboard/> [last accessed on 2022-09-26].

Camelyon17 In medical applications, the goal is to apply models trained on a comparatively small set of hospitals to a larger number of hospitals. For this application, we study images of tissue slides under a microscope to determine whether a patient has cancer or not. Shifts in patient populations, slide staining, and image acquisition can impede model accuracy in previously unseen hospitals. Camelyon17 comprises images of tissue patches from five different hospitals. While the first three hospitals are the source domains (302,436 examples), the fourth and fifth are the validation (34,904 examples) and test domain (85,054 examples), respectively.

We strictly follow the specifications made in (Koh et al., 2021) using DenseNet-121 (Huang et al., 2017) as the feature extractor, a learning rate of $10e-3$, an L_2 regularization of $10e-2$, a batch size of 32, and stochastic gradient with momentum of 0.9. We trained for 5 epochs using early stopping.

We deviate from the specifications made in (Koh et al., 2021) in terms of the FE. We use the FE from Feng et al. (2020); Peng et al. (2019) since we observed a higher mean accuracy and faster training than with the by Koh et al. (2021) originally proposed DenseNet-121 FE (Huang et al., 2017). We trained the FE from scratch. Both, ERM and the DG were trained over 250 epochs with early stopping, a learning rate of 0.001, which is reduced by a factor of 0.2 if the cross-entropy loss has not improved after 10 epochs. All results were aggregated over ten runs.

FMoW Analyzing satellite images with machine learning (ML) models may enable novel possibilities in tackling global sustainability and economic challenges such as population density mapping and deforestation tracking. However, satellite imagery changes over time due to human behavior (e.g., infrastructure development), and the extent of change is different in each region. The Functional Map of the World (FMoW) dataset consists of satellite images from different continents and years: training (76,863 images; between 2002–2013), validation (19,915 images; between 2013 and 2016), and test (22,108 images, between 2016–2017). The objective is to determine one of 62 building types (e.g., shopping malls) and land-use.

As instructed in Koh et al. (2021), we used the DenseNet-121 (Huang et al., 2017) pre-trained on ImageNet without L_2 -regularization. For the optimization, we use the Adam optimizer with a learning rate of $1e-4$, which is decayed by a factor of 0.96 per epoch. The models were trained for 50 epochs with early stopping and a batch size of 64. Additionally, we report the worst-region accuracy, which is a specific metric used for FMoW. This worst-region accuracy reports the worst accuracy across the following regions: Asia, Europe, Africa, America, and Oceania (see Koh et al. (2021) for the details). Again, we report the results over three runs.

Amazon Recent research shows that consumer-facing machine learning application large performance disparities across different set of users. To study this performance disparities, WILDS (Koh et al., 2021) leverages a variant of the Amazon Review dataset. The Amazon-WILDS dataset is composed of data from 3,920 domains (number of reviewers) and the task is a multi-class sentiment classification, where the model receives a review text and has to predict the rating from one to five. To split this dataset, a between training, validation, and test disjoint set of reviewers is used: training (245,502 reviews from 1,252 reviewers), validation (100,050 reviews from 1,334 reviewers), test (100,050 reviews from 1,334 reviewers).

For the experiments and baseline models, we use the specifications made in Koh et al. (2021). As for the FE, we used DistilBERT-base-uncased models (Sanh et al., 2020). For ERM, we use a batch size of 8, learning rate $1e-5$, L_2 regularization of 0.01, 3 epochs with early stopping and 512 as the maximum length of tokens.

For training the Gated Domain layer, we used the same specifications as made for ERM. The performance is measured in 10th percentile accuracy.

iWildsCam Wildlife camera traps offer an excellent possibility to understand and monitor biodiversity loss. However, images from different camera traps differ in illumination, color, camera angle, background, vegetation, and relative animal frequencies. We use the iWildsCam dataset consisting of 323 different camera traps positioned in different locations worldwide. In the dataset, we refer to different locations of camera traps as different domains, in particular 243 training traps (129,809 images), 32 validation traps (14,961 images), and 48 test traps (42,791 images). The objective is to classify one of 182 animal species.

Following the instructions by Koh et al. (2021), we used again the ResNet50 pre-trained on ImageNet (He et al., 2016). For ERM, we used a learning rate of $3e-5$ and no L2-regularization. The models were trained for 12 epochs with a batch size of 16 with the Adam optimizer. In addition to the accuracy, we report the macro F1-score to evaluate the performance on rare species (see Koh et al. (2021) for details). All results were aggregated over three runs.

RxRx1 In biomedical research areas such as genomics or drug discovery, high-throughput screening techniques generate a vast amount of data in several batches. Because experimental designs cannot fully mitigate the effects of confounding variables like temperature, humidity, and measurements across batches, this creates heterogeneity in the observed datasets (commonly known as batch effect). The RxRx1 dataset comprises images obtained by fluorescent microscopy from 51 domains (disjoint experiments): training (40,612 images, 33 domains), validation (9,854 images, 4 domains), and test (34,432 images, 14 domains). The aim is to classify one of 1,139 genetic treatments. All results were aggregated over three runs.

We conducted the RxRx1 experiments in accordance with the specifications made in (Koh et al., 2021). As for the FE, we, thus, used the ResNet50 pre-trained on ImageNet (He et al., 2016). We trained the models using AdamW with default parameters $\beta_1 = 0.9$ and $\beta_2 = 0.999$ using a learning rate of $1e-4$ and a L2-regularization with strength $1e-5$ for 90 epochs with a batch size of 75. We scheduled the learning rate to linearly increase in the first ten epochs and then decreased it following a cosine rate. For training the Gated Domain layer, we chose the same parameters as for the ERM. All results were aggregated over three runs.

OGB-MolPCBA In biomedical research, machine learning has the potential to accelerate drug discovery while reducing the experimental overhead due to lowering the number of experiments required. However, to leverage the potential of machine learning, the models need to generalize to molecules structurally different from those seen during training. To study this OOD generalization across molecule scaffolds, we use the OGB-MolPCBA dataset. This dataset is split into the following subsets according to the scaffold structure: training (44,930 domains), validation (31,361 domains), and test (43,739 domains). The task is to classify the presence/absence of 128 biological activities based on a graph representation of a molecule.

In line with Koh et al. (2021), we use a Graph Isomorphism Network (GIN) combined with virtual nodes (GIN-virtual; Xu et al. (2019) and Gilmer et al. (2017)) as the FE. For training ERM and our DG, we use the default parameters: five GNN layers with a dimensionality of 300 and a learning rate of 0.001. We train for 100 epochs using early stopping. As for the performance, we report the mean and standard deviation of the average precision across all scaffolds (domains) over three runs.

CivilComments In the last decades, users have generated a vast amount of text on the Internet, some of which contain toxic comments. Machine learning has been leveraged for automatic text review to flag toxic comments. However, the models are prone to learn spurious correlations between toxicity and information on demographics in the comment, which causes the model performance to drop in specific subpopulations. To study this OOD task, we leverage the modified CivilComment dataset from Koh et al. (2021). Based on text input, the task is to predict a binary label, toxic or non-toxic. The domains are defined according to eight demographic identities: male, female, LGBTQ, Christian, Muslim, other religions, Black, and White. All comments were randomly split into a disjoint training (269,038 comments), validation (45,180 comments), and test (133,782 comments) set.

Again, we follow Koh et al. (2021) and use a DistillBERT-base-uncased model (Sanh et al., 2020) with the following parameters: batch size = 16, learning rate = 1e-5, AdamW optimizer, number of epochs = 5, L2 regularization 0.01, and the maximum number of tokens of 300. We use these default parameters for training our Gated Domain layer. The performance is measured in the worst-group accuracy and we report mean and standard deviation across five runs.

PovertyMap As the FMoW example shows, satellite images in combination with machine learning models can be used to monitor sustainability and economic challenges on a global scale. Another application of these satellite images is poverty estimation across different spatial regions. However, there exists a lack of labels for developing countries since obtaining the ground truth is expensive, which makes this application attractive for machine learning models. To study the OOD generalization to unseen countries, we use a modified version of the poverty mapping dataset of WILDS (Koh et al., 2021). The task is to predict a real-valued asset wealth index between 1 and 5 based on a multi-spectral satellite image. The domain refers to the country and whether the the the image is from a rural or urban are. In contrast to the other datasets, this dataset is split in five different folds, whereby in each fold the the training, validation and test set contains a disjoint set of countries, however, data from both rural and urban regions. The average size of each set across the 5 folds is for the training ~10,000 images (13-14 countries), ~4,000 images (4-5 different countries), and for the test set ~4,000 images (13-14 countries).

We follow Koh et al. (2021) and use a pre-trained ResNet-18 model minimizing the squared error loss. For the optimization, we rely on the Adam optimizer with the following parameters: learning rate of 1e-3 with a decay of 0.96 per epoch, batch size of 64 and early stopping based on the OOD evaluation score. For evaluation, we report the Pearson correlation (r) between the predicted and actual asset wealth indices across the five different folds.

Table 8: Parameters for Gated Domain layer in WILDS experiments for the Fine Tuning (FT) and End-to-end training (E2E) Settings.

EXPERIMENT			M	N	λ_{L_1}	λ_{OLS}	λ_{ORTH}	σ	κ
WILDS BENCHMARK	FT AND E2E	CS	5	10	$1e^{-3}$	$1e^{-3}$	-	4	2
		MMD	5	10	$1e^{-3}$	$1e^{-3}$	-	4	2
		PROJECTION	5	10	-	$1e^{-3}$	$1e^{-3}$	16	-

On the challenge of obtaining domain labels. In the example of hospitals (e.g. Camelyon17 dataset), domain labels come, in fact, for free. However, other examples, such as the CivilComments dataset, show the opposite. This dataset requires additional annotations (i.e., demographic identities), which can be tedious to obtain in practice. Some algorithms need these domain annotations to achieve superior performance on each subgroup. Furthermore, the task of subgroup detection in itself is a difficult and relevant problem. Coming back to our hospital example, even people from the same hospital might belong to different subpopulation (e.g. gender, race, age) and these demographic subgroups are often more relevant for diagnosis than which hospital a patient comes from. This information, however, is not always available (due to anonymization standards, for instance) and, therefore, the relevant domain annotation might be hard to obtain.

General benchmark methods Following the WILDS benchmarking procedure (Koh et al., 2021), we compare our proposed Gated Domain layer to the following baselines. First, empirical risk minimization (ERM), which minimizes the average training loss over the pooled dataset. Second, a group of DG algorithms provided by the WILDS benchmark, namely, Coral, Fish, IRM, and DRO. The Coral algorithm introduces a penalty for differences in means and covariances of the domains feature distributions. The Fish algorithm achieves DG by approximating an inter-domain gradient matching objective, i.e., maximizing the inner product between gradients from different domains (Shi et al., 2021). Conceptually, Fish learns feature representations that are invariant across domains. Invariant risk minimization (IRM) introduces a penalty for feature distributions with different optimal classifiers for each domain (Arjovsky et al., 2019). The idea is to enable OOD generalization by learning domain-invariant causal predictors. Lastly, group distributionally robust optimization (DRO) explicitly minimizes the training loss on the worst-case domain (Sagawa et al., 2020; Hu et al., 2018).

In addition to the baselines originally presented in Koh et al. (2021), we consider the following more recent DG baselines. First, we describe LISA, which instead of regularizing the internal representations for generalization, seeks to learn domain-invariant predictors with selective data augmentation Yao et al. (2022). Common Gradient Descent (CGD), introduced by Piratla et al. (2022), is based on Group-DRO. However, it proposes to focus not on groups with the worst regularization but on common groups that enable generalization. Last, Adaptive Risk Minimization using batch normalization (ARM-BN) by Zhang et al. (2021) is different from the methods presented since it adapts to previously unseen domains during test time using unlabeled observations from this test domain.